Title

Smoothened determines β-arrestin–mediated removal of the G protein–coupled receptor Gpr161 from the primary cilium

Journal

Journal of Cell Biology, 212(7)

ISSN

0021-9525

Authors

Pal, Kasturi
Hwang, Sun-hee
Somatilaka, Bandarigoda
et al.

Publication Date

2016-03-28

DOI

10.1083/jcb.201506132

Peer reviewed

Smoothened determines β-arrestin–mediated removal of the G protein–coupled receptor Gpr161 from the primary cilium

Kasturi Pal,[1] Sun-hee Hwang,[1] Bandarigoda Somatilaka,[1] Hemant Badgandi,[1] Peter K. Jackson,[2] Kathryn DeFea,[3] and Saikat Mukhopadhyay[1]

[1]Department of Cell Biology, University of Texas Southwestern Medical Center, Dallas, TX 75390
[2]Department of Microbiology and Immunology, Stanford University School of Medicine, Stanford, CA 94305
[3]Division of Biomedical Sciences, University of California, Riverside, Riverside, CA 92521

Dynamic changes in membrane protein composition of the primary cilium are central to development and homeostasis, but we know little about mechanisms regulating membrane protein flux. Stimulation of the sonic hedgehog (Shh) pathway in vertebrates results in accumulation and activation of the effector Smoothened within cilia and concomitant disappearance of a negative regulator, the orphan G protein–coupled receptor (GPCR), Gpr161. Here, we describe a two-step process determining removal of Gpr161 from cilia. The first step involves β-arrestin recruitment by the signaling competent receptor, which is facilitated by the GPCR kinase Grk2. An essential factor here is the ciliary trafficking and activation of Smoothened, which by increasing Gpr161–β-arrestin binding promotes Gpr161 removal, both during resting conditions and upon Shh pathway activation. The second step involves clathrin-mediated endocytosis, which functions outside of the ciliary compartment in coordinating Gpr161 removal. Mechanisms determining dynamic compartmentalization of Gpr161 in cilia define a new paradigm for down-regulation of GPCRs during developmental signaling from a specialized subcellular compartment.

Introduction

The primary cilium is a specialized apical compartment that functions as a signaling antenna by preferentially localizing select components, particularly during sonic hedgehog (Shh) signaling in vertebrates. Interestingly, Shh pathway regulators are remarkably dynamic in cilia. Upon Shh treatment, Smoothened (Smo), a frizzled family seven-transmembrane receptor that functions as the major transducer of Shh signaling accumulates in cilia (Corbit et al., 2005). Simultaneously, Patched (Ptch1; the Shh receptor) and a recently identified negative regulator, the orphan G protein–coupled receptor (GPCR), Gpr161, both of which normally localize to cilia, are lost from the compartment (Rohatgi et al., 2007; Mukhopadhyay et al., 2013). An increasing number of other rhodopsin family GPCRs are being reported to localize to cilia (Berbari et al., 2008a,b; Marley and von Zastrow, 2010; Loktev and Jackson, 2013; Marley et al., 2013; Koemeter-Cox et al., 2014; Omori et al., 2015). Selective trafficking (Nachury et al., 2007; Berbari et al., 2008b; Mukhopadhyay et al., 2010; Sun et al., 2012) and retention mechanisms regulate ciliary GPCR pools (Hu et al., 2010; Francis et al., 2011; Garcia-Gonzalo et al., 2011; Chih et al., 2012; Reiter et al., 2012). However, factors down-regulating GPCRs from ciliary membrane are unknown.

The pathways for removal of GPCRs from the plasma membrane are well characterized and occur through the agonist-induced process of "desensitization." Upon agonist binding, phosphorylation by GPCR kinases (GRKs) result in interactions with β-arrestins (Benovic et al., 1985, 1987; Luttrell and Lefkowitz, 2002; Gurevich and Gurevich, 2006; Moore et al., 2007). Simultaneously, β-arrestins function as scaffolds for the clathrin machinery to induce endocytosis (Goodman et al., 1996; Moore et al., 2007; Marchese et al., 2008). However, the primary cilia must depend on other mechanisms or at least on modifications of the β-arrestin/clathrin-based mechanism for GPCR removal. First, endocytic vesicles are not observed in the primary cilium and are found only in association with a specialized region of membrane near the base of the compartment, called the ciliary pocket (Rohatgi and Snell, 2010; Benmerah, 2013). Second, although the ciliary membrane is an extension of the plasma membrane, membrane barriers (Hu et al., 2010)

Correspondence to Saikat Mukhopadhyay: saikat.mukhopadhyay@utsouthwestern.edu

Abbreviations used in this paper: BiFC, bimolecular fluorescence complementation; BRET, bioluminescence resonance energy transfer; CAMYEL, conformation-based cAMP BRET biosensor; Chc, clathrin heavy chain; CK1α, casein kinase 1α; CLS, ciliary localization sequence; GPCR, G protein–coupled receptor; Gpr161, G protein–coupled receptor 161; Grk, GPCR kinase; MEF, mouse embryonic fibroblast; Ptch1, Patched; SAG, Smoothened agonist; Shh, Sonic hedgehog; Smo, Smoothened; WT, wild type.

The Rockefeller University Press $30.00
J. Cell Biol. Vol. 212 No. 7 861–875
www.jcb.org/cgi/doi/10.1083/jcb.201506132

and a transition zone at the base restrict the ciliary compartment from the apical membrane (Reiter et al., 2012). Finally, no agonist has been identified for Gpr161, which appears to be constitutively active for cAMP signaling (Mukhopadhyay et al., 2013). Defining the trafficking mechanisms that regulate Gpr161 flux provides the unique opportunity to identify mechanisms underlying dynamic regulation of GPCRs in cilia. Here, we describe molecular mechanisms determining removal of Gpr161 from cilia, which establishes a novel paradigm for GPCR down-regulation during development.

Results

Disappearance of Gpr161 from cilia depends on its constitutive signaling activity

It is possible that Shh pathway ligands directly activate Gpr161 to trigger its loss from cilia. Using a cAMP biosensor-based assay, we determined that Shh pathway agonists do not act as Gpr161 ligands (Fig. S1 A). Thus, we wondered whether the constitutive activity of Gpr161 was required for its disappearance from cilia. To test this, we introduced a single mutation in the second intracellular loop of Gpr161 (V158E, following the "D[E]RY" motif) that completely prevents constitutive cAMP production (Fig. 1 A; Mukhopadhyay et al., 2013). Mutant and wild-type (WT) GFP-tagged Gpr161 fusions were stably expressed in NIH 3T3 Flp-In fibroblasts. Because overexpression of GPCRs can artifactually elongate cilia, thereby compromising Shh pathway activation, we meticulously screened these and all other stable lines for Smo trafficking and levels of expression. After treating these stable cells with the Smo agonist SAG to activate the Shh pathway, we quantified the percentage of GFP-positive cilia by immunofluorescence. WT $Gpr161^{GFP}$ was completely lost from cilia within 4 h of SAG treatment (Fig. 1, B and C; and Fig. S1 B), recapitulating disappearance of endogenous Gpr161 from cilia upon Shh signaling in kidney IMCD3 cells (Mukhopadhyay et al., 2013). However, the $Gpr161^{V158E}$ mutant was retained in the cilia upon SAG treatment (Fig. 1, B and C; and Fig. S1 C). Importantly, the $Gpr161^{V158E}$ mutant did not affect Smo trafficking to cilia (Fig. S1 D), ensuring ciliary integrity. In addition, expression of the Gpr161 fusions was comparable (Fig. S1 E). Thus, disappearance of Gpr161 from cilia requires its constitutive activity.

Basal and Shh-regulated Gpr161 ciliary pools depend on β-arrestins

Active GPCRs are desensitized by recruitment of β-arrestins, which terminate receptor signaling (Moore et al., 2007; Marchese et al., 2008). β-Arrestins have been previously reported to localize to cilia (Kovacs et al., 2008; Molla-Herman et al., 2010) (Fig. S1 F). To examine the role of β-arrestins in removal of Gpr161 from cilia, we used *β-arrestin1/2* single- and double-knockout primary mouse embryonic fibroblasts (MEFs). In WT and single-knockout MEFs, endogenous Gpr161 is efficiently lost from cilia within 2 h of treatment with Shh (Fig. 1 D and Fig. S1, G and H). In contrast, in *β-arrestin1/2* double-knockout MEFs, the disappearance of Gpr161 from cilia upon Shh signaling was completely abrogated (Fig. 1 D and Fig. S1, G and H). Thus, Shh-dependent Gpr161 loss from cilia is dependent on the combined activity of both β-arrestins. We also noted that the degree of localization of Gpr161 to cilia in untreated *β-arrestin* double-knockout MEFs was increased to ∼80% compared with ∼30% for WT and single knockout MEFs (Fig. 1 D and Fig. S1, G and H). These data indicate that basal Gpr161 levels in cilia are also regulated by β-arrestins.

Signaling-competent Gpr161 binds to β-arrestins

GPCR–β-arrestin interactions are often transient, and we were unable to detect Gpr161-β-arrestin binding using coimmunoprecipitation assays, as reported recently (Feigin et al., 2014). Instead, we tested for Gpr161–β-arrestin interactions in vivo using intermolecular bioluminescence resonance energy transfer (BRET) ratiometric assays. These assays are effective in determining transient protein-protein interactions in live cells quantitatively (Hamdan et al., 2006; Pfleger and Eidne, 2006). Nonciliated T-REx-293 cells were cotransfected with Rluc–β-arrestin1/2 and Gpr161-eYFP fusions. As Gpr161 demonstrates constitutive activity, we titrated $Gpr161^{WT}$-eYFP and $Gpr161^{V158E}$-eYFP levels by transfecting increasing concentrations against a constant amount of Rluc–β-arrestin1/2. Specific protein–protein interactions result in a saturable increase in BRET ratio with increasing eYFP acceptor levels, as the binding sites in the luciferase donor are completely occupied. In contrast, a linear rise in BRET ratio with increasing acceptor/donor ratios indicates nonspecific binding (Hamdan et al., 2006; Pfleger and Eidne, 2006). We observed a saturating BRET signal indicating specific interaction between $Gpr161^{WT}$-eYFP and Rluc–β-arrestin2 and a lower but still concentration-dependent and saturable increase in BRET ratio with Rluc–β-arrestin1 (Fig. 1 E). In both cases, the BRET signals were reduced with the nonsignaling $Gpr161^{V158E}$ mutant (Fig. 1 E), indicating that the β-arrestin interactions are specific and dependent on Gpr161 constitutive activity.

The β-arrestin binding site maps to the proximal C tail of Gpr161

A near-complete deletion of Gpr161 C tail ($Gpr161^{FullCT\text{-}del}$; Fig. 1 A) completely abrogated β-arrestin2 recruitment in the intermolecular BRET assays (Fig. 1 F), similar to the $Gpr161^{V158E}$ mutant (Fig. 1 E), and was retained in cilia upon Shh pathway activation without affecting Smo accumulation (Fig. S1 I). Interestingly, a slightly smaller deletion of the C terminus of Gpr161, which corresponds to the *vacuolated lens* (*vl*) mouse allele (Matteson et al., 2008), increased recruitment of β-arrestin2, compared with the WT receptor (Fig. 1 F). Thus, the major region that binds to β-arrestin2 is the C-terminal tail upstream of the *vl* deletion (377–401 aa).

Steady-state Gpr161 ciliary levels are not controlled by Shh pathway activity

Having established the role of β-arrestin binding, we next examined which aspects of Shh signaling might trigger Gpr161 removal from cilia. Smo undergoes lateral transport in and out of cilia at steady-state (Ocbina and Anderson, 2008; Kim et al., 2009; Milenkovic et al., 2009); however, Shh treatment results in removal of Ptch1 from cilia, and concomitant accumulation of activated Smo (Corbit et al., 2005; Rohatgi et al., 2007). To test which of these events triggered Gpr161 loss (Fig. 2 A), we assessed Gpr161 ciliary levels in *Ptch1* and *Smo* knockout MEFs. Under resting conditions, *Smo* knockout MEFs showed up-regulated steady-state levels of Gpr161 in cilia relative to WT, which remained unchanged upon further Shh pathway

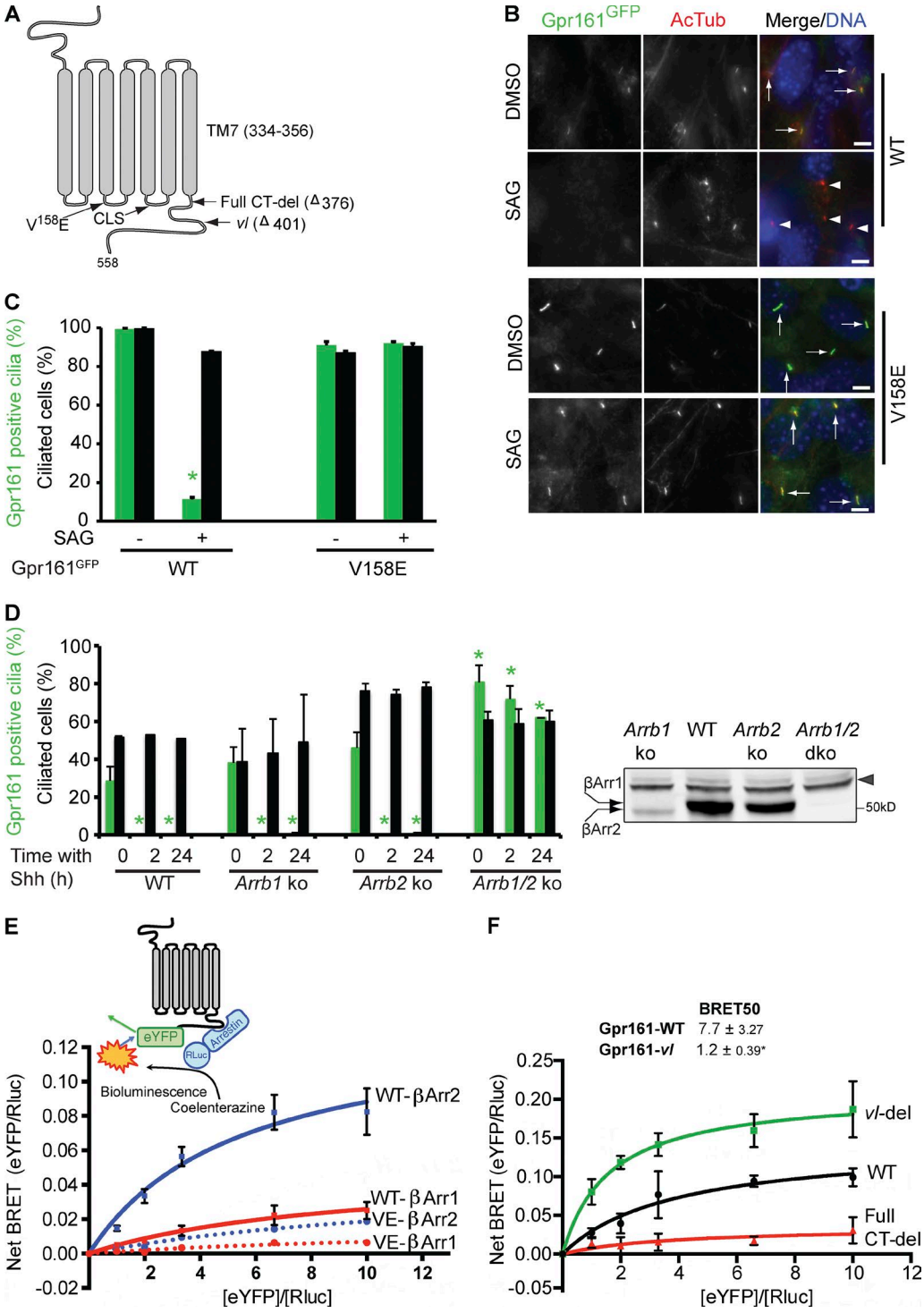

Figure 1. **Ciliary loss of Gpr161 depends on its signaling activity and direct binding to β-arrestins.** (A) Cartoon representing mutations in mouse Gpr161 (NP_001074595.1). CLS, ciliary localization signal (Mukhopadhyay et al., 2013); Δ, deletion of the C tail; CT, C terminus. (B and C) Confluent NIH 3T3 Flp-In cells stably expressing GFP-tagged WT and full-length *Gpr161* mutant (V158E) were starved for 24 h, treated ±SAG (500 nM) for the last 4 h before fixing, and immunostained with anti-GFP (green) and anti–acetylated tubulin (AcTub; red) antibodies. Arrows and arrowheads indicate cilia positive and negative for Gpr161, respectively. All images were imported from ImageJ using similar parameters. Bar, 5 µm. Data represent mean ± SD from three independent experiments (C). *, $P < 0.0001$ with respect to untreated WT *Gpr161*. (D) Confluent WT, *β-arrestin1* (*Arrb1*), *β-arrestin2* (*Arrb1*), and *β-arrestin1/2* double-knockout MEFs (*Arrb1/2* ko) were serum starved for 48 h, treated ±Shh (300 ng/ml) for the indicated time points before fixation, and immunostained with anti-Gpr161 and anti–acetylated tubulin antibodies. Data represent mean ± SD from two independent experiments. *, $P < 0.0001$ with respect to untreated WT cells. Untreated whole-cell lysates immunoblotted with anti–β-arrestin (A1CT) antibody are shown to the right (arrowhead, nonspecific band). (E and F) T-REx 293 cells cotransfected with a constant amount of Rluc-tagged *β-arrestin1/2* (donor) and increasing amounts of eYFP-tagged WT or indicated *Gpr161* mutants (acceptor) were incubated with coelenterazine-h (5 µM) for 10 min. Readings were taken using the 475- and 535-nm emission filters simultaneously to compute net BRET ratios (Materials and methods). Total DNA transfected was maintained constant by transfecting empty vector. $BRET_{50}$ values are shown above (Materials and methods). Data represent mean ± SD from three independent experiments. *, $P = 0.01$ with respect to only Gpr161/β-arrestin2 cotransfected cells. See also Fig. S1.

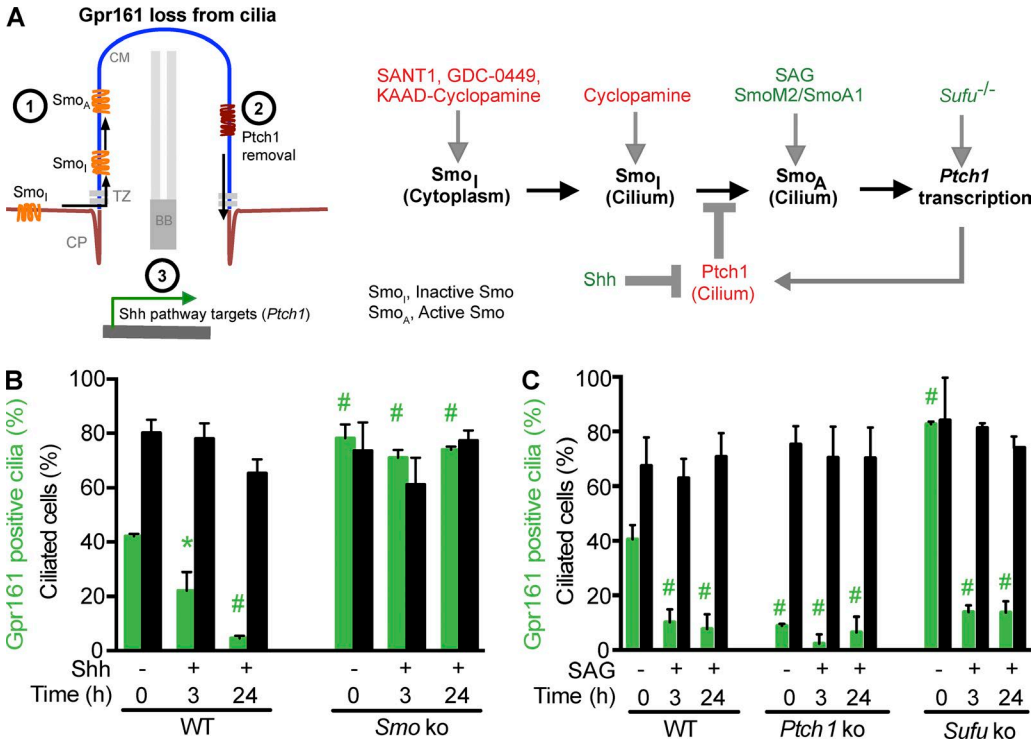

Figure 2. **Steady-state localization of Gpr161 in cilia is not controlled by Shh pathway activity.** (A) Alternative models for Shh pathway activation-mediated Gpr161 loss from cilia: accumulation of Smo, removal of Ptch1, or downstream activation of pathway targets (left). Cartoon showing regulation of Smo trafficking to cilia by Smo antagonists (right; adapted partly from Rohatgi et al., 2009). *Sufu*$^{-/-}$ MEFs show increased Ptch1 levels in cilia (Fig. S2 E). (B and C) Confluent WT, *Smo*$^{-/-}$, *Ptch1*$^{-/-}$ or *Sufu*$^{-/-}$ MEFs were serum starved for 48 h, treated ±500 nM SAG or 300 ng/ml octyl-Shh for the indicated time periods before fixation, and immunostained using anti-Gpr161 and anti–acetylated tubulin antibodies. Quantification of Gpr161-positive cilia from two independent experiments (mean ± SD). *, P < 0.05; #, P < 0.01 with respect to untreated WT cells in each panel. See also Fig. S2.

activation (Fig. 2 B and Fig. S2, A and B). In contrast, Gpr161 was constitutively absent from the cilia in *Ptch1* knockout MEFs (Figs. 2 C and S2 C). This effect could be caused by increased Shh pathway activity or accumulation of activated Smo in cilia as a consequence of lack of Ptch1 (Rohatgi et al., 2009). To distinguish between these possibilities, we examined *Sufu* knockout MEFs, which like *Ptch1* knockouts show increased Shh signaling, albeit by different mechanisms (Fig. 2 A). The absence of Sufu causes decreased stability of Gli family transcriptional effectors (Chen et al., 2009; Humke et al., 2010; Tukachinsky et al., 2010), increased *Ptch1* transcripts (Svärd et al., 2006) and resting Ptch1 levels in cilia (Fig. S2 E). However, upon SAG treatment, Smo accumulates in cilia in *Sufu* knockouts (Tukachinsky et al., 2010). In contrast to *Ptch1* knockouts, in *Sufu* knockout MEFs the steady-state levels of Gpr161 in the cilia were dramatically increased and Gpr161 was rapidly removed upon SAG treatment (Figs. 2 C and S2 D). Together, these data suggest that Gpr161 cilia levels are not controlled by Shh signaling per se; rather, ciliary levels of Gpr161 are negatively correlated with either the presence of Smo or the lack of Ptch1 in cilia. Moreover, they demonstrate that, like Smo (Ocbina and Anderson, 2008; Kim et al., 2009; Milenkovic et al., 2009), steady-state levels of Gpr161 in cilia reflect a constant flux of entry and exit.

Presence of activated Smo in cilia determines steady-state levels of Gpr161

To further investigate if either Smo accumulation or Ptch1 removal resulted in Gpr161 disappearance from cilia, we perturbed Smo flux through cilia by treatment with Smo antagonists and tested basal levels of ciliary Gpr161 in resting WT MEFs. Small-molecule inhibitors of Smo, such as KAAD-cyclopamine, GDC-0449, and SANT1, completely prevent Smo trafficking to cilia, whereas cyclopamine causes Smo to accumulate in cilia in an inactive state (Chen et al., 2009; Rohatgi et al., 2009; Wilson et al., 2009; Fig. 2 A). Upon inhibiting Smo trafficking to cilia by KAAD-cyclopamine, GDC-0449, and SANT1 in WT resting MEFs, Gpr161-positive cilia increased to ∼80%, suggesting that ciliary pools of Smo negatively regulate basal levels of Gpr161 (Figs. 3 A and S3 A). Importantly, treatment of *Ptch1*$^{-/-}$ MEFs with SANT1, which reduces ciliary accumulation of Smo in the *Ptch1* knockout (Rohatgi et al., 2009), also resulted in increased basal levels of Gpr161 to ∼80% (Figs. 3 B and S3 B). Thus, Smo ciliary accumulation, and not Ptch1 removal, most directly correlates with Gpr161 loss from cilia.

Cyclopamine results in ciliary accumulation of inactive Smo, unlike KAAD-cyclopamine (Chen et al., 2009; Rohatgi et al., 2009; Wilson et al., 2009; Kim et al., 2014). Interestingly, basal levels of Gpr161 in resting WT MEFs were unaffected upon treatment with cyclopamine (Figs. 3 A and S3 A). Simultaneous treatment with SANT1 prevents accumulation of Smo in cyclopamine-treated cells (Rohatgi et al., 2009) and resulted in increased Gpr161 localization to cilia (Figs. 3 A and S3 A). Because inactive Smo also traffics in and out of the cilia at steady-state, it accumulates in the cilia of *dynein 2* knockout MEFs, which are defective in retrograde intraflagellar transport (Ocbina and Anderson, 2008; Kim et al., 2009; Milenkovic et al., 2009). As in cyclopamine-treated cells, and unlike *Ptch1* knockouts, we did not detect any changes in basal levels of ciliary Gpr161 in the *dynein 2* heavy-chain knockout (*Dync2h1*$^{lln/lln}$)

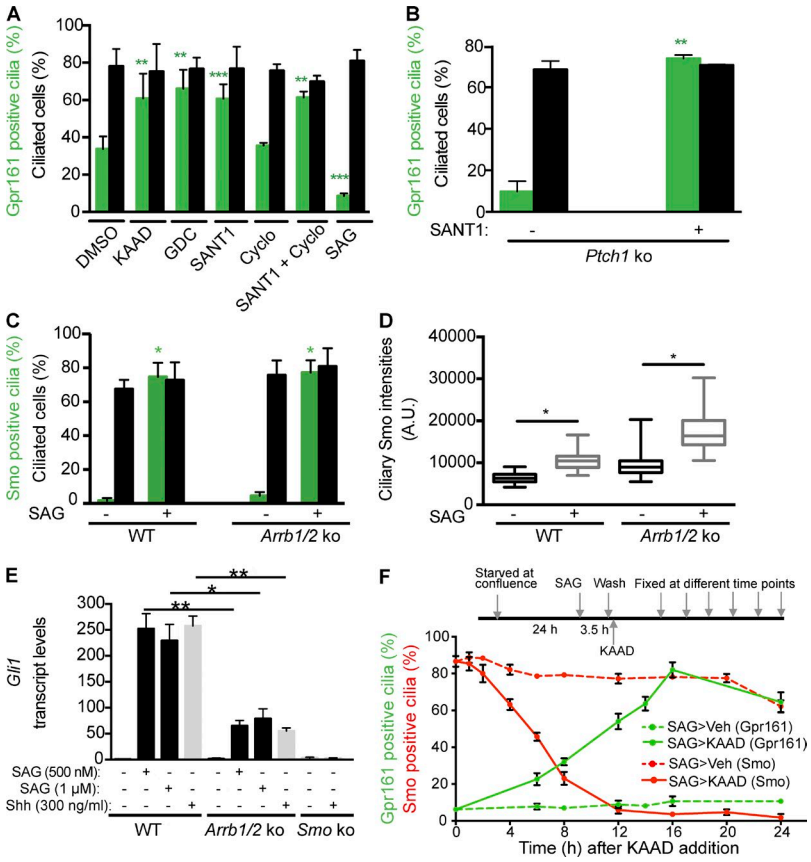

Figure 3. **Presence of activated Smo in cilia determines steady-state levels of Gpr161.** (A) Confluent WT MEFs were serum starved for 48 h, treated ±drugs for 24 h before fixation, and immunostained as in Figure 2 (B and C). Drugs used were as follows: 500 nM SAG, 1 µM KAAD-cyclopamine (KAAD), 1 µM GDC-0449 (GDC), 1 µM SANT1, and 5 µM cyclopamine (cyclo). Data represent mean ± SD from at least three independent experiments. **, $P < 0.01$; ***, $P < 0.001$ with respect to DMSO-treated cells. (B) Confluent *Ptch1*$^{-/-}$ MEFs were serum starved for 48 h, treated ±1 µM SANT1 for the last 24 h before fixation, and processed as in A. Quantification from two independent experiments (mean ± SD). **, $P < 0.01$ with respect to untreated cells. (C and D) Confluent WT and *β-arrestin1/2* double-knockout MEFs (*Arrb1/2* ko) were serum starved for 48 h, treated ±1 µM SAG in starvation media for 36 h before fixation, and immunostained using anti-Smo and anti–acetylated tubulin antibodies. Quantification from two independent experiments (mean ± SD) in C. Pixel intensities of Smo levels in cilia were determined by immunofluorescence (D); A.U., arbitrary units of fluorescence; $n \geq 43$ each. *, $P < 0.001$ with respect to untreated cells in each background in C and D. (E) Confluent WT, *Arrb1/2* double-knockout, or *Smo* knockout MEFs were starved for 18 h and further treated ± SAG/Shh for 30 h in starvation medium. Total RNA was isolated, and *Gli1* expression levels were determined by quantitative real-time RT-PCR. Data represent mean ± SD from three experiments. *, $P < 0.05$; **, $P < 0.01$. (F) Confluent IMCD3 Flp-In cells were starved for 24 h. Next, cells were treated with 500 nM SAG for 3.5 h in starvation media, washed, and further treated ±1 µM KAAD-cyclopamine (KAAD) in starvation media before fixing. Cells were processed for Gpr161- and Smo-positive cilia by immunofluorescence. SAG>Veh and SAG>KAAD denotes pretreatment with SAG and subsequent treatment with vehicle (DMSO) or KAAD-cyclopamine, respectively. Data represent mean ± SD from three experiments for Gpr161 quantification and three fields from one experiment for Smo quantification. See also Fig. S3.

MEFs compared with WT (Fig. S3 C). Retrograde intraflagellar transport by dynein 2 is required for both Smo activation and flux of activated Smo in cilia (Ocbina and Anderson, 2008; Kim et al., 2009, 2014). We did not see a further decrease in ciliary levels of Gpr161 upon Shh pathway activation in *Dync2h1*$^{lln/lln}$ MEFs (Fig. S3 C). Overall, we conclude that the accumulation of active Smo in cilia regulates the steady-state levels of Gpr161.

It is possible that retention of Gpr161 in cilia upon Shh pathway activation in *β-arrestin* double knockouts results from lack of Smo trafficking to cilia, rather than a direct effect as we have proposed (Kovacs et al., 2008). However, ciliary accumulation of endogenous Smo in the *β-arrestin* double-knockout MEFs upon SAG treatment was similar to WT (Fig. 3, C and D; and Fig. S3 D). Thus, β-arrestin–regulated disappearance of Gpr161 from cilia is not because of impaired Smo trafficking. We consistently noted a ∼60% decrease in up-regulation of *Gli1* levels in *β-arrestin* double-knockout MEFs upon Shh pathway activation (Fig. 3 E). This reduction in Shh signaling was partially rescued upon siRNA-mediated *Gpr161* knockdown, despite incomplete knockdown in the primary double-knockout MEFs (Fig. S3 E). Thus, ciliary retention of Gpr161 causes decreased Shh signaling in *β-arrestin* double-knockout MEFs, irrespective of Smo trafficking to cilia.

Gpr161 disappearance from cilia is reversible

Recycling of GPCRs to the plasma membrane after agonist-induced endocytosis regulates GPCR function (Lefkowitz et al., 1998; Tanowitz and von Zastrow, 2003). Based on our understanding of Smo flux regulating Gpr161 pools in cilia, we tested for the reversibility of its ciliary loss. Confluent IMCD3 cells were initially starved for 24 h to induce full ciliation and subsequently treated with SAG to remove endogenous Gpr161 from cilia. After washing off SAG, we measured for endogenous ciliary pools after treatment with KAAD-cyclopamine. KAAD-cyclopamine prevents basal Smo entry and should competitively inhibit any residual SAG by binding to the same ligand pocket in Smo (Ruat et al., 2014). Ciliary levels of Gpr161 fully recovered in cells treated with KAAD-cyclopamine, but after a long time course ($t_{1/2}$ = 10 h), and this was preceded by Smo disappearance from cilia ($t_{1/2}$ = 5 h; Figs. 3 F and S3 F). The timeline of Gpr161 recovery is much slower than the timeline for its disappearance upon Shh signaling ($t_{1/2}$ = 30 min; Fig. S1 B; Mukhopadhyay et al., 2013). In cells treated with vehicle only, Smo was retained in cilia even after washing, likely because of residual bound SAG, and Gpr161 levels did not recover (Fig. 3 F). Thus, the ciliary loss of Gpr161 is reversible.

Smo enhances recruitment of β-arrestins by Gpr161

To determine the mechanism by which activated Smo triggers Gpr161 removal from cilia, we tested if Smo regulates β-arrestin recruitment by Gpr161. Smo has been previously shown to recruit β-arrestins (Kovacs et al., 2008; Chen et al., 2011). Interestingly, in intermolecular BRET assays, exogenous Smo expression significantly enhanced interaction between

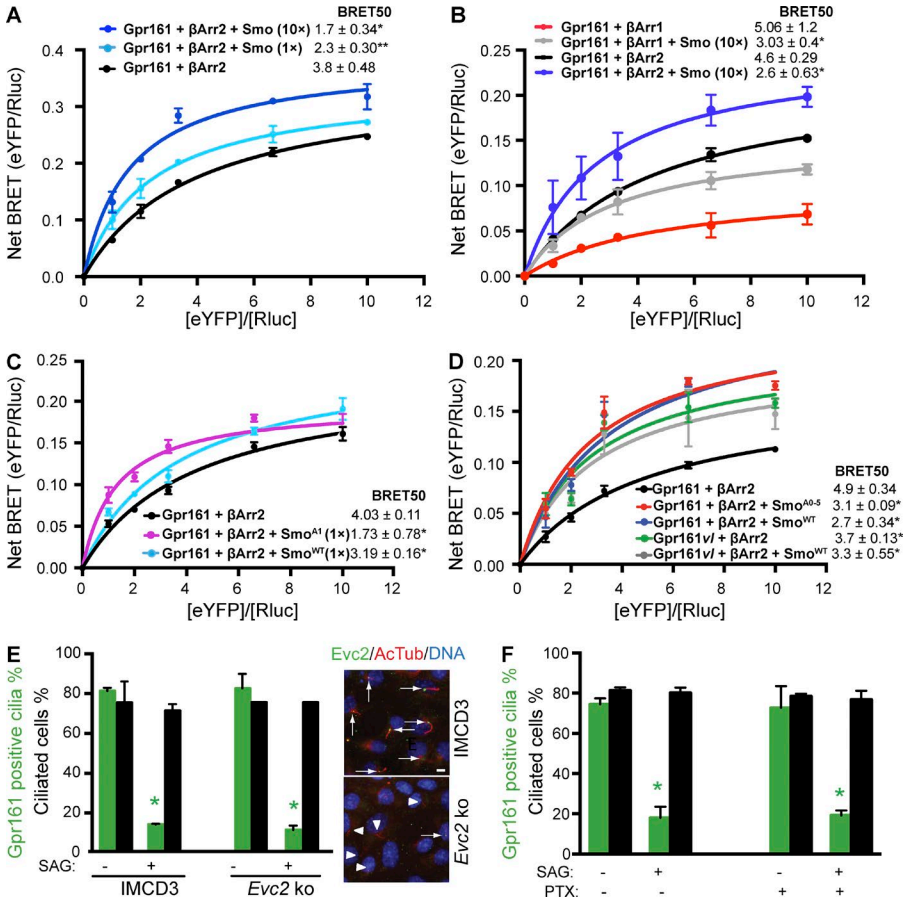

Figure 4. **Smo enhances recruitment of β-Arrestin to Gpr161.** (A–D) T-REx 293 cells were cotransfected with a constant amount of Rluc–β-arrestin1/2 (donor) and increasing amounts of Gpr161-eYFP or Gpr161^{vl}-eYFP (acceptor), ± untagged human Smo (0.1 µg/well of a six-well plate, 1×; 1 µg/well of a six-well plate, 10×; A and B) or mouse Smo^{WT}-Myc, Smo^{A1}-Myc or Smo^{A0-5}-Myc (0.1 µg each/well of a six-well plate, 1× in C; 1 µg/well of a six-well plate, 10× in D). Cells were subjected to BRET analysis (Materials and methods). The titration curves are mean ± SEM from three independent experiments in all panels. *, $P < 0.05$; **, $P < 0.01$ for $BRET_{50}$ values with respect to only Gpr161/β-arrestin2 cotransfected cells in each panel. Total DNA transfected was maintained constant by transfecting empty vector. (E) IMCD3 Flp-In cells were knocked out for *Evc2* using CRISPR/Cas9 genome editing technology. Confluent cells were starved ±250 nM SAG for the last 24 h before fixing and immunostained to quantify for Gpr161-positive cilia. Data represent mean ± SD from two independent experiments. *, $P < 0.05$ with respect to DMSO-treated cells in each case. Merged images on right show Evc2-positive cilia as assessed by immunofluorescence; 80% ($n = 485$) in WT and 26% ($n = 552$) in *Evc2* knockout. Bar, 5 µm (F) Confluent IMCD3 Flp-In cells were treated ±250 nM SAG ±800 ng/ml pertussis toxin for 24 h in starvation media after reaching confluence, fixed, and immunostained to quantify for Gpr161-positive cilia. Data represent mean ± SD from two independent experiments. *, $P < 0.01$ with respect to DMSO-treated cells in each case. See also Fig. S4.

Gpr161^{WT}-eYFP and either Rluc–β-arrestin1 or Rluc–β-arrestin2 in a concentration-dependent manner (Fig. 4, A and B). Coexpression and activation of other cilia localized GPCRs, such as the dopamine receptor D2R, had no effect on the interaction between β-arrestin2 by Gpr161; thus, the Smo-mediated effect was specific (Fig. S4 A). Coexpression of a constitutively active mouse Smo mutant (SmoA1, similar to human SmoM2; Chen et al., 2011) at a lower concentration resulted in increased binding of β-arrestin2 to Gpr161, relative to WT mouse Smo (Fig. 4 C), demonstrating that activated Smo was more effective.

Smo recruits β-arrestin2 by its C-terminal tail upon phosphorylation by Grk2 and casein kinase 1α (CK1α; Chen et al., 2004, 2011; Meloni et al., 2006; Philipp et al., 2008). β-Arrestin2 recruitment by Smo and transfer to Gpr161 in the membrane milieu could be a mechanism for enhanced β-arrestin2 binding to Gpr161. However, exogenous expression of a nonphosphorylated form of mouse Smo (Smo^{A0-5}), which is incapable of interacting with β-arrestin2 (Chen et al., 2011), was also able to enhance recruitment of β-arrestin2 by Gpr161 (Fig. 4 D). To determine if downstream effectors of Smo regulate Gpr161 loss from cilia, we tested if Evc/Evc2 complex (Dorn et al., 2012) and $G\alpha_i$ regulate this process (Ogden et al., 2008). However, Gpr161 loss upon SAG treatment was not affected in *Evc2* knockouts (Fig. 4 E), similar to knockdown of another recently identified Smo effector, *Dlg5* (Chong et al., 2015). In addition, pretreatment with pertussis toxin (to inhibit $G\alpha_i$) had no effect on preventing either Smo-mediated β-arrestin2 recruitment to Gpr161 in intermolecular BRET titration assays (Fig. S4 B) or Gpr161 loss from cilia (Fig. 4 F). Furthermore, inhibition of Gβγ-mediated signaling in cilia, by transfecting a ciliary-targeted Grk2 C-terminal fusion that sequesters these subunits (Koch et al., 1994), did not inhibit SAG-mediated removal of Gpr161 from IMCD3 cilia (Fig. S4 D). Thus, Smo-mediated enhancement of β-arrestin2 binding to Gpr161 is not related to the β-arrestin2 binding ability of Smo or known downstream effectors.

Loss of Gpr161 from cilia is dependent on Grk2

GRKs regulate phosphorylation of activated GPCRs and recruitment of β-arrestins (Moore et al., 2007). Upon efficient siRNA-mediated knockdown of individual *Grks* in IMCD3 cells, we found that knockdown of *Grk2* completely prevented Gpr161 removal from cilia (Fig. 5 A). Smo phosphorylation by Grk2 and CK1α regulates its trafficking to the cilia (Chen et al., 2011). However, Smo accumulation in cilia was not affected upon *Grk2* knockdown alone, suggesting that Gpr161 removal was not a consequence of impaired Smo trafficking (Figs. 5 B and S4 E). In addition, the Smo phosphorylation mutant enhanced β-arrestin2 recruitment to Gpr161, similar to wild type Smo (Fig. 4 E). To determine if the role of Grk2 in Gpr161 removal was direct, and not an indirect consequence of its role in phosphorylating other cellular targets (Pitcher et al., 1998; Ferreira et al., 2012), we generated two *GRK2* CRISPR knockout cell lines in T-REx-293 cells and tested for β-arrestin recruitment using intermolecular BRET assays. Upon acute inhibition of remaining *GRK2* using a specific inhibitor (paroxetine; Thal et al., 2012; Homan et al., 2014), β-arrestin2 recruitment to

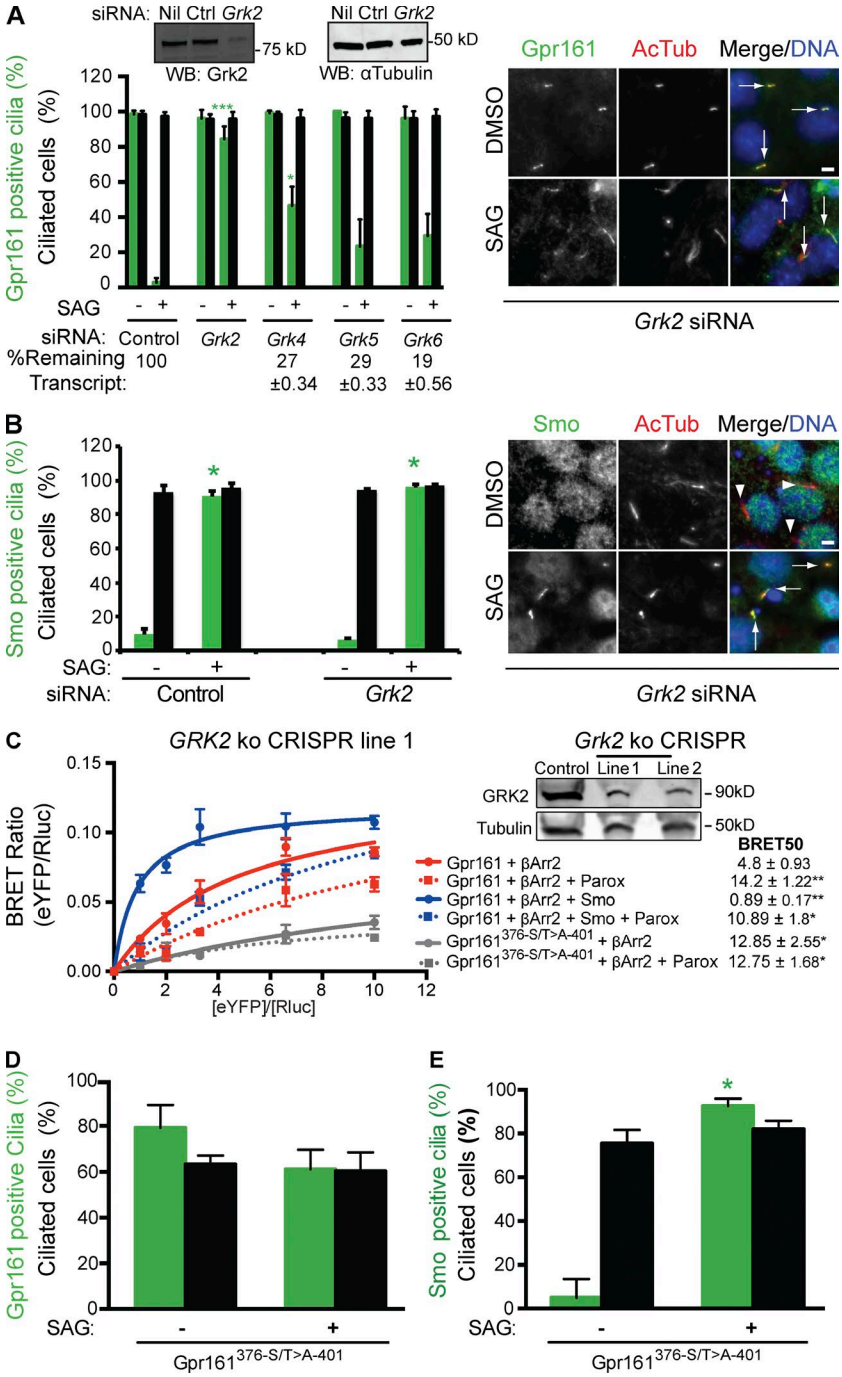

Figure 5. **The GPCR kinase Grk2 determines removal of Gpr161 from cilia by inhibiting β-arrestin binding to the receptor.** (A and B) IMCD3 Flp-In cells were reverse transfected with siRNA against indicated *Grks* for 72 h. Confluent cells were starved for the last 24 h ±250 nM SAG before fixing and processed for immunofluorescence using anti-Gpr161/Smo and anti–acetylated tubulin antibodies to quantify cilia positive for Gpr161/Smo by microscopy. Data represent mean ± SD from four independent experiments (A) and three separate fields from one experiment (B). *, P < 0.01; ***, P < 0.0001 with respect to SAG-treated control (ctrl) siRNA-treated cells (A); *, P < 0.0001 with respect to untreated cells in each condition (B). Inset in A shows the efficiency of *Grk2* knockdown as assessed by immunoblotting. "% Remaining" siRNA (mean ± SD) for respective genes with respect to control siRNA-treated cells by quantitative real-time RT-PCR is shown at the bottom for *Grk4-6*. Arrows refer to Gpr161- or Smo-positive cilia, and arrowheads denote Smo-negative cilia. Bar, 5 µm. (C) *GRK2* knockout (ko) lines in T-REx 293 cells were generated using CRISPR technology. Knockout lines were cotransfected with a constant amount of Rluc–β-arrestin2 (donor) and increasing amounts of eYFP-tagged *Gpr161* WT or phosphosite mutant (acceptor) ±1 µg untagged human *Smo* per well of a six-well plate. The phosphosite mutant (C–E) constitutes mutating seven S/T to A in the C tail of full-length *Gpr161* (376–401 aa; 376-E**S**FVQRQRT**S**RLF**S**I**S**NRI**T**-DLGL**S**P-401). Cells were subjected to BRET analysis (Materials and methods) after pretreatment ±50 µM paroxetine (a selective GRK2 inhibitor) for 1 h (Thal et al., 2012; Homan et al., 2014). The titration curves are mean ± SD from two independent experiments. Efficiency of *GRK2* knockouts as assessed by immunoblotting is shown to the top right. BRET assays performed in knockout line 2 are shown in Fig. S4 C. *, P < 0.05; **, P < 0.01 with respect to Rluc–β-arrestin2 binding to Gpr161-eYFP. (D and E) Confluent NIH 3T3 Flp-In cells stably expressing GFP-tagged *Gpr161* phosphosite mutant were starved ±1 µM SAG, fixed, and processed for immunofluorescence and microscopy for Gpr161/Smo and acetylated tubulin. Bar, 5 µm. Data represent mean ± SD from two independent experiments (D) and three separate fields from one experiment (E). *, P < 0.001 with respect to untreated cells. See also Fig. S4.

Gpr161 was reduced with respect to untreated cells, irrespective of the presence of Smo (Figs. 5 C and S4 C). Thus, Grk2 directly functions in β-arrestin recruitment by Gpr161. Based on the β-arrestin binding site in Gpr161 (376–401 aa; Fig. 1 E) we generated a full-length *Gpr161* mutant with all the putative S/T sites in this region mutated to alanines. In stable NIH 3T3 Flp-In cell lines expressing the phosphosite mutant, removal from cilia was abrogated, although Smo accumulation in cilia remained unaffected (Fig. 5, D and E). Recruitment of β-arrestin2 by the phosphosite mutant was also reduced, compared with WT receptor (Fig. 5 C). Furthermore, acute inhibition of remaining GRK2 using paroxetine did not further reduce recruitment of β-arrestin2 in the *GRK2* knockout T-REx-293 cells, suggesting that the GRK2 phosphorylation sites map to the mutated S/T sites (Fig. 5 C). Thus, Grk2 directly regulates β-arrestin recruitment by Gpr161 and its removal from cilia.

The *vacuolated lens* truncated Gpr161 mutant is retained in cilia

β-Arrestin binding was increased in the Gpr161^{vl} mutant compared with the WT receptor, irrespective of Smo (Figs. 1 F and 4 D). However, upon generating a stable line with equivalent levels of expression to the WT fusion in NIH 3T3 Flp-In cells, the Gpr161^{vl}-GFP mutant localized normally to the cilia but was retained upon SAG treatment (Figs. 6 A and S5 B). Smo trafficking to cilia was not affected, ensuring ciliary integrity (Fig. S5 A). Therefore, in addition to the Gpr161 proximal C tail (376–401 aa) that regulates its disappearance from cilia

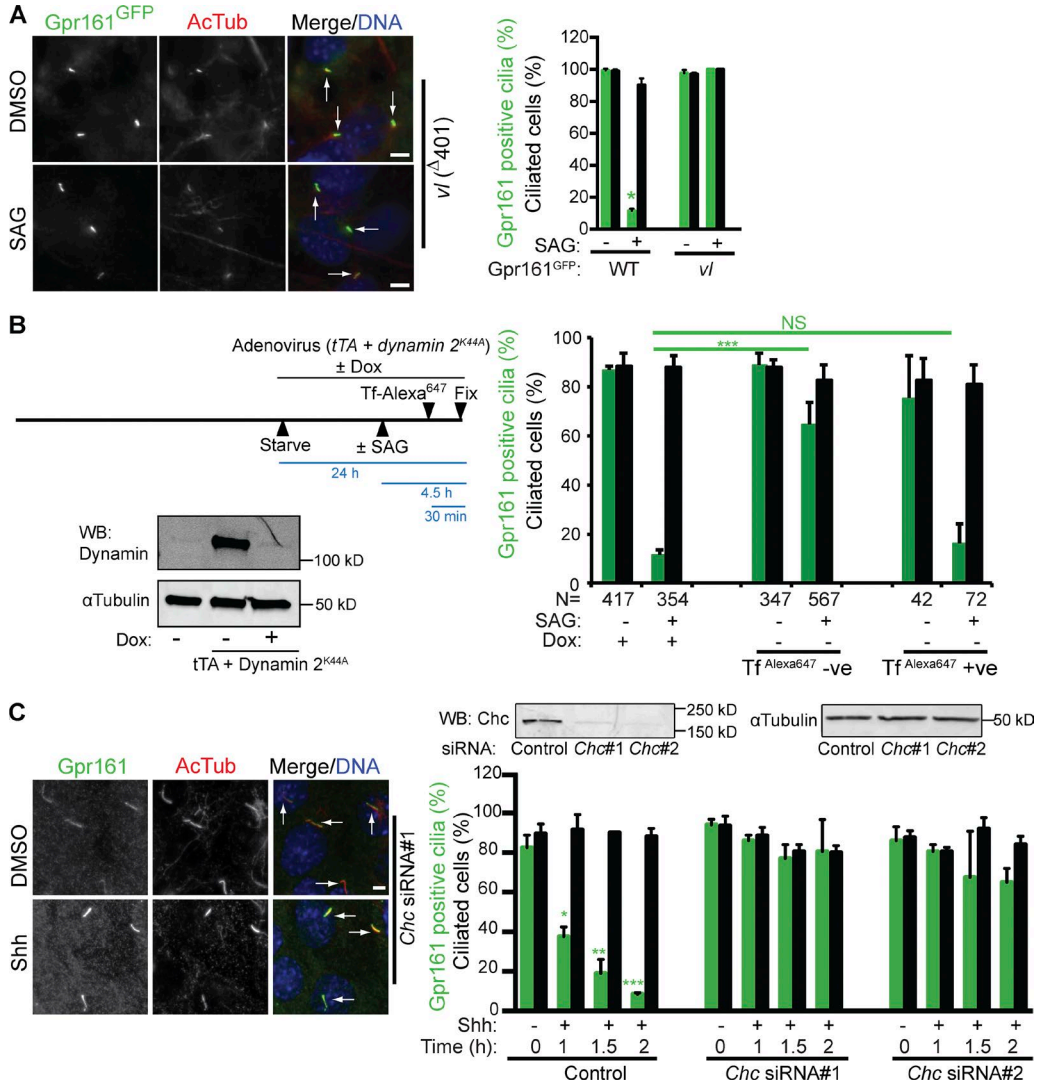

Figure 6. **Disappearance of Gpr161 from cilia is dependent on clathrin-mediated endocytosis.** (A) Confluent NIH 3T3 Flp-In cells stably expressing GFP-tagged *vl* truncation of *Gpr161* were starved for 24 h, treated ±500 nM SAG for the last 4 h before fixing and immunostained with anti-GFP (green) and anti–acetylated tubulin (AcTub; red) antibodies. All images were imported from ImageJ using similar parameters as in Fig. 1 B. Bar, 5 µm. Quantification from three independent experiments shown to the right (mean ± SD); *, $P < 0.01$ with respect to untreated GFP-tagged WT *Gpr161*. (B) IMCD3 Flp-In cells were infected with adenoviruses expressing *dynamin* 2^{K44A} and tetracycline transactivator (*tTA*) in starvation media (±10 ng/ml doxycycline [Dox]) and treated ±250 nM SAG for the last 4.5 h before fixing (top left). Simultaneous treatment with 50 µg/ml transferrin-Alexa^{647} (Tf-Alexa^{647}) for the last 30 min was used to estimate for dynamin inhibition. Fixed cells were processed for immunofluorescence for Gpr161 and acetylated tubulin. Overall efficiency of dynamin2 overexpression was also assessed by immunoblotting (left). Data represent mean ± SD from three independent experiments. ***, $P < 0.0001$; NS, not significant; N, total number of cells counted. (C) IMCD3 Flp-In cells were transfected with siRNAs against clathrin heavy chain (*Chc*) for 72 h. Confluent cells were starved for the last 24 h, treated with 30 ng/ml Shh for the indicated time periods before fixing, and processed for immunofluorescence for Gpr161 (green) and acetylated tubulin (red). Data represent mean ± SD from two independent experiments. *, $P < 0.01$; **, $P < 0.001$; ***, $P < 0.0001$ with respect to untreated control siRNA-treated cells. Inset shows the efficiency of *Chc* knockdown as assessed by immunoblotting. Representative images after 2 h of Shh treatment are shown to the left. Arrows indicate cilia positive for Gpr161 (A and C). Bar, 5 µm. See also Fig. S5.

by β-arrestin binding (Fig. 1 F and Fig. 5, C–E), the distal C terminus of the receptor (402–558 aa) also determines ciliary loss. The ciliary retained *vl* mutant allowed us to directly test for Gpr161^{vl}–β-arrestin binding inside the ciliary compartment. We used a bimolecular fluorescence complementation (BiFC) assay by fusing complementary halves of eVenus to the binding partners (Kodama and Hu, 2010). We detected robust fluorescence complementation inside IMCD3 cilia, suggesting that these proteins interact in this compartment (Fig. S4 F). The interaction was specific, as the nonbinding Gpr161^{V158E} mutant, in contrast to Gpr161^{vl}, did not show significant complementation, even with a ciliary-targeted β-arrestin2 fusion (Fig. S4 G). Thus, the Gpr161^{vl} mutant is retained in cilia, despite efficient β-arrestin binding in the compartment.

Loss of Gpr161 from cilia is dependent on clathrin-mediated endocytosis

β-Arrestins act as cytosolic scaffolds for the clathrin-mediated endocytosis machinery (Goodman et al., 1996; Luttrell and Lefkowitz, 2002; Moore et al., 2007; Marchese et al., 2008). Interestingly, Ptch1 removal from cilia upon Shh treatment is mediated by caveolar-type endocytosis (Yue et al., 2014). As dynamins mediate multiple types of endocytic pathways (Doherty and McMahon, 2009), we first inhibited dynamins

by infecting IMCD3 cells with adenovirus expressing a doxycycline-repressible dominant negative mutant *dynamin 2*^{K44A} (Damke et al., 1995). Simultaneously, we estimated cellular dynamin inhibition by fluorescent transferrin uptake (Fig. 6 B). Expression of *dynamin 2*^{K44A} prevented endogenous Gpr161 disappearance from cilia upon SAG treatment. However, infected cells that did not exhibit dynamin inhibition lost Gpr161 upon SAG treatment (Fig. 6 B). Thus Gpr161 disappearance from cilia is regulated by endocytosis.

To determine the mechanism of endocytosis regulating Gpr161 disappearance from cilia, we tested for the role of clathrin. Upon efficient siRNA-mediated knockdown of the clathrin heavy chain (*Chc*), loss of Gpr161 from cilia in Shh-treated IMCD3 cells was completely inhibited (Fig. 6 C). Importantly, ciliary accumulation of Smo upon pathway activation was intact (Fig. S5, C and D). Clathrin has additional functions in trafficking of proteins from trans-Golgi to the endosomal compartment (Bonifacino and Lippincott-Schwartz, 2003). However, Gpr161 ciliary levels in resting cells were not affected upon clathrin knockdown (Fig. 6 C), suggesting that clathrin is not required for preciliary trafficking. Finally, a C-terminal fusion of the C tail of Gpr161 (357–558 aa) with the extracellular and transmembrane domain of CD8α, but not with the third intracellular loop of Gpr161, was endocytosed from the surface of ARPE-19 cells upon addition of an anti-CD8 antibody (Fig. S5 F). Importantly, endocytosis of the C tail fusion was inhibited upon siRNA-mediated knockdown of clathrin heavy chain (Fig. S5 F). This suggests that the C tail of Gpr161 regulates scaffolding with the clathrin-mediated endocytosis machinery. Clathrin is localized outside cilia at the ciliary pocket (Fig. S5 E; Rohatgi and Snell, 2010; Benmerah, 2013). Overall, Gpr161 loss from cilia is dependent on clathrin-mediated endocytosis that functions outside of the ciliary compartment.

We next determined if the lack of removal of Gpr161 has an effect on Shh signaling in the C-terminal mutants. We generated multiple stable lines in NIH 3T3 cells overexpressing either WT or mutant forms of untagged Gpr161 in equivalent levels. We detected a consistent decrease in *Gli1* levels upon addition of SAG in the β-arrestin binding site mutant (376–401 aa, S/T>A), with respect to the *vl* mutant (Fig. S5 G). Although, ciliary retention of Gpr161 and Smo trafficking to the compartment upon Shh pathway activation are equivalent between the two C-terminal mutants (Fig. 5, D and E; Fig. 6 A; and Fig. S5 A), β-arrestins bind significantly better to the *vl* truncation compared with the WT (Figs. 1 F and 4 D) and bind poorly to the 376–401 aa S/T>A mutant (Fig. 5 C). Thus, reduced cAMP/protein kinase A (PKA) signaling resulting from β-arrestin–mediated desensitization in the *vl* truncation mutant possibly prevents suppression of Shh signaling. Overall, ciliary retention of Gpr161 in *β-arrestin* double knockouts (Figs. 3 E and S3 E) and of the β-arrestin binding site mutant receptor results in decreased Shh signaling irrespective of Smo trafficking to the compartment.

Discussion

Factors regulating disappearance of Gpr161 from cilia

Basal or Shh-regulated Gpr161 ciliary pools are determined by the following obligatory factors: (a) β-arrestins binding only to the signaling-competent receptor inside cilia, (b) Grk2-mediated recruitment of β-arrestin to the proximal C tail of the receptor, (c) trafficking/activation of Smo in cilia that increases β-arrestin recruitment to the receptor, and (d) subsequent clathrin-mediated endocytosis outside cilia (Fig. 7). Interestingly, Gpr161 loss from cilia is determined by coopting β-arrestin recruitment, which is enhanced by Smo. β-Arrestin2 has recently been reported to determine removal of the somatostatin receptor Sstr3 from cilia upon treatment with ligands (Green et al., 2015). Known Shh pathway agonists do not directly regulate Gpr161 cAMP signaling. Although, we cannot rule out endogenous ligands that could result in receptor activation, based on the enhancement of β-arrestin1/2 recruitment by Smo, we favor the model that Gpr161 removal is primarily regulated by activated Smo levels in cilia. In addition, Gpr161 removal is regulated by both β-arrestins, unlike Sstr3.

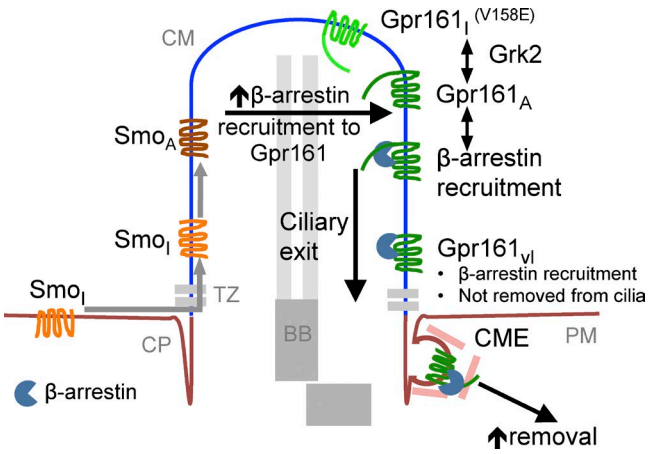

Figure 7. **Mechanism of Gpr161 loss from cilia.** Model for Gpr161 loss from cilia (Discussion). Abbreviations: BB, basal body; CP, ciliary pocket; CM, ciliary membrane; Gpr161$_A$, signaling-competent Gpr161; Gpr161$_I$, inactive Gpr161; PM, plasma membrane; Smo$_I$, inactive Smo; Smo$_A$, Smo in active conformation; TZ, transition zone.

Ciliary entry and activation of Smo, rather than Ptch1 removal or Shh pathway activity, directly reduce Gpr161 ciliary pools. Increased Shh pathway activity through terminal transcriptional effectors does not directly impact on Gpr161 ciliary pools, as Gpr161 ciliary levels are dramatically opposite in *Ptch1* and *Sufu* knockouts. Although both Ptch1 and Gpr161 are lost from the cilia upon Shh treatment, Ptch1 removal occurs independent of Gpr161 loss. First, Ptch1 levels in cilia do not directly drive Gpr161 loss, as treatment with SANT1 (that inactivates and prevents Smo ciliary entry) results in Gpr161 accumulation in cilia of *Ptch1* knockouts. Second, Ptch1 removal from cilia upon Shh signaling is proposed to be caveolin mediated (Yue et al., 2014), whereas clathrin-mediated endocytosis determines Gpr161 loss. Instead, Smo trafficking into cilia directly correlates with Gpr161 loss. Even in resting cells, the addition of Smo antagonists that prevent Smo entry into cilia increases basal Gpr161 ciliary pools. Smo accumulates in an inactive state in cilia upon treatment with the Smo antagonist cyclopamine and in *dynein 2* knockout MEFs. In these conditions, ciliary levels of Gpr161 are similar to untreated WT MEFs, unlike *Ptch1* knockout MEFs, suggesting that Smo activation in cilia is critical for reducing Gpr161 levels.

Gpr161 disappearance from cilia is also regulated by clathrin-mediated endocytosis outside cilia. First, Gpr161 is retained along with Smo in cilia upon clathrin knockdown and

dynamin inhibition. Second, the Gpr161^{vl} mutant with deletion of the distal C tail binds to β-arrestins efficiently but is not lost from cilia. As the C tail fusion of Gpr161 is endocytosed in a clathrin-dependent manner, the most parsimonious model would be that receptor tail regulates efficient β-arrestin scaffolding with the clathrin-mediated endocytosis machinery. As Gpr161 accumulates in cilia despite clathrin localization outside of this compartment, we propose that a juxtaciliary membrane barrier limits diffusion of Gpr161 into the rest of the apical plasma membrane (Vieira et al., 2006; Lu et al., 2015), and endocytosis occurs at this membrane domain.

Smo increases β-arrestin binding to Gpr161

Using intermolecular BRET assays for quantitatively measuring Gpr161–β-arrestin binding in vivo, we demonstrate that Smo expression results in increased β-arrestin recruitment by Gpr161 in a concentration- and activation-dependent manner. Thus, Smo effectively functions as a "coreceptor" in modulating Gpr161's β-arrestin binding capacity. Gpr161 removal from cilia and Gpr161–β-arrestin binding are not regulated by known downstream effectors of Smo (Ogden et al., 2008; Dorn et al., 2012; Chong et al., 2015). A β-arrestin nonbinding Smo mutant (Smo$^{A0\text{-}5}$) is equally effective as WT in enhancing β-arrestin recruitment to Gpr161, suggesting this process to be independent of Smo–β-arrestin binding and Smo phosphorylation by Grk2/CK1α (Meloni et al., 2006; Philipp et al., 2008; Chen et al., 2011). Interestingly, *Grk2* knockdown prevents Gpr161 loss from cilia without affecting Smo accumulation in cilia, and Gpr161–β-arrestin2 interactions are GRK2 dependent, likely through phosphorylation of the proximal C tail. Alternatively, direct Smo-Gpr161 interactions could stabilize β-arrestin binding to Gpr161. β-Arrestin–GPCR interactions are typically initiated by destabilization of the β-arrestin polar core upon binding to phosphorylated residues in GPCRs and final occupancy of the receptor interhelical cavity by flexible β-arrestin loops (Gurevich and Gurevich, 2006; Shukla et al., 2014). The Gpr161^{vl} mutant also results in increased β-arrestin recruitment, irrespective of Smo. This suggests that the Gpr161 distal C tail may have an inhibitory role in preventing maximal β-arrestin recruitment by Gpr161. Smo might prevent functioning of this inhibitory domain and/or stabilize β-arrestin binding to Gpr161 at the interhelical cavity.

Shh-dependent loss of Gpr161 from cilia could be because of decreased entry into cilia and/or increased removal. The rate of Gpr161 trafficking into cilia, as measured by recovery of ciliary pools after loss, is much slower than the timeline for its disappearance from cilia upon Shh signaling, indicating increased removal. The reciprocal flux of Smo and Gpr161 ordinarily suggests only a "window" of opportunity for Smo to promote Gpr161 removal. However, there is continuous flux of Smo in resting cilia and upon Shh signaling (Milenkovic et al., 2009; Kim et al., 2014). β-Arrestins form multimeric complexes with the anterograde intraflagellar transport motor Kif3a and Smo upon Shh pathway activation (Kovacs et al., 2008), and Smo exit from cilia in SAG-activated cilia is dynein 2 dependent (Kim et al., 2014); thus, Gpr161 exit might use similar pathways.

Gpr161 ciliary retention is associated with reduced Shh signaling

We consistently noted a decrease in *Gli1* levels upon Shh pathway activation in *β-arrestin* double-knockout MEFs and upon stable overexpression of the β-arrestin binding site *Gpr161* mutant (376–401 aa, S/T>A) with respect to the *vl* truncation. Interestingly, the suppression of Shh signaling in *β-arrestin* double-knockout MEFs was not because of a lack of endogenous Smo trafficking to cilia, as previously reported for overexpressed Smo (Kovacs et al., 2008). Lack of suppression of Shh signaling in the *vl* truncation upon overexpression and in mouse models (Matteson et al., 2008; Li et al., 2015) is possibly related to reduced cAMP/PKA signaling consequent upon increased β-arrestin binding. Interestingly, increased Gpr161 ciliary accumulation in *Inpp5e* knockouts is also associated with decreased Shh signaling (Garcia-Gonzalo et al., 2015) and reduced hippocampal neurogenesis (Chávez et al., 2015). However, although Gpr161 is retained in cilia upon *Grk2* knockdown, *Grk2* knockout embryos show minor impact on neural tube patterning (Philipp et al., 2008). Dorsoventral neural tube patterning is predominantly dependent on the Gli2 activator (Persson et al., 2002; Goetz and Anderson, 2010) and is less sensitive to partial reduction in pathway activity (Li et al., 2011). A knockin version of the cilia-retained receptor expressed in endogenous levels, and not compromised in cAMP/PKA signaling, would be required to conclusively determine the effects of Gpr161 ciliary retention upon Shh signaling. We predict that decreased Shh pathway activity upon Gpr161 ciliary retention would affect tissues regulated by high signaling, such as during proliferation of the external granule progenitors in the neonatal cerebellum and in hippocampal neurogenesis.

Materials and methods

Antibodies and reagents

An affinity-purified rabbit polyclonal antibody against a C-terminal peptide (mouse Gpr161; Cys-RGSRTLVNQRLQLQSIKEGNVLAAEQR-COOH) of Gpr161 was remade with YenZym as described previously (Mukhopadhyay et al., 2013). Gifts of rabbit polyclonal antibodies are as follows: anti-GFP (J. Seeman, University of Texas Southwestern Medical Center, Dallas, TX), anti-Ptch1 (R. Rohatgi, Stanford University, Palo Alto, CA), anti-Smo (K. Anderson, Memorial Sloan Kettering Cancer Center, New York, NY), anti–pan-β-arrestin A1CT used in immunoblotting (R. Lefkowitz, Duke University, Durham, NC), and anti-Evc2 (V.L. Ruiz-Perez, Consejo Superior de Investigaciones Científicas, Autonomous University of Madrid, Madrid, Spain). Commercial antibodies used were against α-tubulin (clone DM1A, T6199; Sigma-Aldrich; and YL1/2; Thermo Fisher Scientific), acetylated α-tubulin (mAb 6-11B-1; Sigma-Aldrich; and rabbit polyclonal 5335; Cell Signaling Technology), CHC (TD.1; Santa Cruz Biotechnology, Inc.), Arl13b (mouse monoclonal N295B/66; NeuroMab), anti–pan-β-arrestin (PA1-730, used in immunofluorescence; Thermo Fisher Scientific), CD8 (C7423; Sigma-Aldrich), CHC (ab21679; Abcam; Watanabe et al., 2014), Dynamin (610245; BD), and Grk2 (sc-562; Santa Cruz Biotechnology, Inc.). Fluorescent secondary antibodies for immunofluorescence were from Jackson ImmunoResearch Laboratories, Inc., whereas IRDye 680RD and IRDye 800CW secondary antibodies for immunoblotting were from Li-COR Biosciences. SAG, Cyclopamine, KAAD-Cyclopamine, SANT-1, and purmorphamine were from EMD Millipore, whereas GDC-0449 was from Cayman Chemicals. Oxysterols were obtained from Avanti Polar Lipids (7-keto-27-hydroxycholesterol, 7α,25-dihydroxycholesterol) or Sigma-Aldrich (20α–hydroxycholesterol). Quinpirole was from Tocris Bioscience. Forskolin, IBMX, pertussis toxin (P2980), paroxetine, and most other reagents were from Sigma-Aldrich. Octyl-Shh has been described previously (Taylor et al., 2001).

Plasmids

Plasmids used were as follows: pG-LAP5 (pEFα-X-Speptide-PrecissionS-EGFP; Torres et al., 2009), Addgene; CAMYEL (R. Taussig and P. Sternweis, University of Texas Southwestern Medical Center, Dallas, TX; Jiang et al., 2007); mouse Smo-Myc and untagged human Smo (L. Lum, University of Texas Southwestern Medical Center, Dallas, TX); Smo-non-phosphomutant (J. Jiang, University of Texas Southwestern Medical Center, Dallas, TX; Chen et al., 2011); Flag-D2R (M. von Zastrow, University of California, San Francisco, San Francisco, CA; Marley and von Zastrow, 2010); and Rluc–β-arrestin1/2 (M. Bouvier, University of Montreal, Montreal, Canada; Pal et al., 2013). Gpr161 (NM_001081126.1) and deletion entry clones were engineered by PCR amplification and subsequent BP recombination reaction into pDONR (Invitrogen). C-terminal expression constructs for Gpr161 were generated by Gateway cloning into pG-LAP5 and for retroviral infections into a gatewaytized LAP5 version of pBAB EPuro. Single or multiple amino acid mutations in full-length Gpr161 were generated using Quikchange site-directed mutagenesis kit (Agilent Technologies) or Phusion high-fidelity DNA polymerase (New England Biolabs, Inc.). Gpr161 phosphosite mutant was generated by synthesizing a S/T>A mutated SacI fragment of the open reading frame of mouse Gpr161 cDNA (1087–1376 bp; NM_001081126.1; GeneArt; Thermo Fisher Scientific), and subsequently cloning into the WT cDNA. $Gpr161^{WT}$-eYFP and $Gpr161^{mutant}$-eYFP constructs were generated by subcloning Gpr161 (WT and V158E mutant) in the eYFP-N1 vector (Takara Bio, Inc.) using HindIII–BamH1 restriction sites. Ciliary-targeted Grk2 C-terminus fusion (ciliary localization sequence [CLS]-mCherry-Grk2CT) was generated by PCR amplification of the mouse fibrocystin CLS from 1–60 aa and subcloning into the N terminus of the previously reported Cry2-mCherry-Grk2 CT (Addgene; O'Neill and Gautam, 2014) construct using NheI site. C-terminal fusions of the distal C tail of Gpr161 (357–558 aa) or the third intracellular loop of Gpr161 (242–296 aa) with the extracellular and transmembrane domain of human CD8α (1–206 aa of NP_001139345.1, followed by a KRLK linker) was generated by subcloning the PCR-amplified Gpr161 regions into the AflIII–NotI site of a CD8α/LDLR construct from M. Mettlen (University of Texas Southwestern Medical Center, Dallas, TX; Mettlen et al., 2010). The CD8α-Gpr161 fragments were further subcloned into pGLAP5 by gateway technology to generate CD8-Gpr161 fragment-LAP5 fusions. To generate VC155-βarrestin2, the C terminus of eVenus from pBiFC-VC155 (Addgene; Kodama and Hu, 2010) was subcloned into pIC113 by PCR amplifying and substituting the GFP sequence using NheI and HindIII sites. β-Arrestin2, together with the linker sequence (GVT GSMGEKP), was PCR amplified from the previously described Rluc–β-arrestin2 construct and ligated to the pIC113–Venus-C construct using HindIII. To generate the VC155–β-arrestin2-CLS-HA construct, the stop codon in the VC155-βarrestin2 was first mutated to AAG. PCR amplification of the CLS sequence of mouse fibrocystin (1–60 aa) was performed with the HA sequence in the reverse primer and was subcloned in this VC155-βarrestin2 (no stop codon) construct using SalI and ApaI. $Gpr161^{vl}$ and $Gpr161^{WT}$ were first cloned into pBiFC-$VN155^{I152L}$ construct (Addgene; Kodama and Hu, 2010) using SalI–XhoI. As this pBiFC construct had a tag before SalI, which would prevent membrane trafficking of Gpr161 by impacting on the signal sequence, the Gpr161-$VN155^{I152L}$ fusion constructs were further subcloned into pcDNA3.1 using NotI site. Site-directed mutagenesis was performed on the pcDNA3 vector with $Gpr161^{WT}$-$VN155^{I152L}$ to generate $Gpr161^{V158E}$-$VN155^{I152L}$ construct. *Gpr161* untagged constructs were constructed in pBABE puro by subcloning respective WT and mutant receptors into the SnaBI site. All constructs were verified by sequencing.

Cell culture and generation of stable cell lines

T-REx-293 (Invitrogen), IMCD3 Flp-In, and Phoenix A (PhA) cells (National Gene Vector Biorepository) were cultured in DMEM high glucose (Sigma-Aldrich; supplemented with 10% FBS [Sigma-Aldrich], 0.05 mg/ml penicillin, 0.05 mg/ml streptomycin, and 4.5 mM glutamine). NIH 3T3 Flp-In cells (Invitrogen) were grown in DMEM high glucose (supplemented with 10% bovine calf serum [Sigma-Aldrich], 0.05 mg/ml penicillin, 0.05 mg/ml streptomycin, and 4.5 mM glutamine). NIH 3T3 Flp-In cell lines stably expressing wild type/mutant $Gpr161^{GFP}$ (Gpr161 followed by Speptide-PrecissionS-EGFP [LAP5]), and untagged receptor constructs were generated using transfection or retroviral infection and antibiotic selection (Mukhopadhyay et al., 2013). ARPE-19 cells were grown in DMEM F12 (Sigma-Aldrich) media with 10% FBS (Sigma-Aldrich), 0.05 mg/ml penicillin, 0.05 mg/ml streptomycin, and 4.5 mM glutamine. Stable CAMYEL T-REx-293 cells (Invitrogen) inducibly coexpressing untagged mouse Gpr161 were generated by transfection of plasmids and antibiotic selection. Transfection of plasmids was done with either Polyfect (QIAGEN) or Bio-T (BioLand Scientific).

Primary MEFs

$Smo^{-/-}$, *$Ptch^{-/-}$* (J. Kim, University of Texas Southwestern Medical Center, Dallas, TX), *$Sufu^{-/-}$* (R. Toftgård, Karolinska Institute, Solna, Sweden), and WT *βarr1*$^{-/-}$, *βarr2*$^{-/-}$, and *βarr1/2* double-knockout (R. Lefkowitz) primary MEFs were maintained in DMEM high glucose (supplemented with 10% FBS, 0.05 mg/ml penicillin, 0.05 mg/ml streptomycin, 4.5 mM glutamine, and 0.1 mM MEM nonessential amino acid supplement). MEFs were assayed within four or five passages in culture.

siRNA transfection

The siRNAs for mouse *Chc* and *Grks* were predesigned On-target Plus (OTP) siRNA duplexes shown to yield a reduced frequency of off-target effects (GE Healthcare; Jackson et al., 2006). IMCD3 Flp-In cells were passaged on glass coverslips and transfected with 200 nM siRNA using Lipofectamine RNAiMax (Invitrogen). *βarr1/2* double-knockout MEFs were reverse and forward transfected with 200 nm of respective OTP siRNAs on the day of plating and the following day using Lipofectamine RNAiMax or DharmaFECT 1. The OTP siRNA sequences are as follows: *Chc* #1, 5′-GGAAAGCAAUCCAUACAGA-3′; *Chc* #2, 5′-UCAGAAGAAUUGCUGCUUA-3′; *Gpr161* #2, 5′-CGGUGG AGUUUGAUGAGUU-3′; *Grk2* #3, 5′-CCAGAUCUCUUCCAG CCAU-3′; *Grk4* #2, 5′-CAUCAAAGAUCCAAGUAAG-3′; *Grk5* #1, 5′-GGACUUAGUGGCAGAAUAU-3′; *Grk6* #1, 5′-GAGCUUAGC CUACGCCUAU-3′. CHC siRNAs #1 and #2 have been published previously (Bonazzi et al., 2011). OTP nontargeting pool (GE Healthcare) was used as control siRNAs in all experiments.

Generation of CRISPR/Cas9 knockouts

Evc2 knockout IMCD3 Flp-In and *GRK2* knockout T-Rex-293 cells were generated using the CRIPSR/Cas9 genome editing strategy as using the guide sequences described previously (Pusapati et al., 2014; Shalem et al., 2014).

Adenovirus infections

IMCD3 Flp-In cells were infected simultaneously with recombinant adenoviruses encoding dynamin 2^{K44A} (driven by minimal CMV promotor, with *tetO* upstream of the promoter) and tetracycline transactivator in starvation media (±10 ng/ml doxycycline) in individual wells of a 24-well plate as shown in the experimental format in the top left of Fig. 6 B (Damke et al., 1995; Schlunck et al., 2004). Adenoviruses were provided by M. Mettlen.

Quantitative real-time RT-PCR

Total RNA was isolated using GenElute mammalian total RNA purification kit (Sigma-Aldrich) or RNeasy plus kit (QIAGEN) following the manufacturer's protocols. Genomic DNA was eliminated from RNA preparations by DNaseI (Sigma-Aldrich) treatment. One-step cDNA

generation and quantitative real-time RT-PCR was performed using SYBR Green quantitative RT-PCR kit (Sigma-Aldrich) or TaqMan assays as described before (Fig. S5 G; Wen et al., 2010). The qPCR primers used were *GFP*, 5′-AGAACGGCATCAAGGTGAAC-3′ and 5′-TGCTCAGGTAGTGGTTGTCG-3′; *Gli1*, 5′-TACCATGAGCCC TTCTTTAG-3′ and 5′-TCATATCCAGCTCTGACTTC-3′; *Grk2*, 5′-CGATACTTCTACTTGTTCCC-3′ and 5′-TCTGGATCACTATCA CACTG-3′; *Grk4*, 5′-TAACCATAATGAATGGAGGGG-3′ and 5′-ATA TTCTCTGGCTTTAGGTCTC-3′; *Grk5*, 5′-TAGAAGACTTACACC GTGAG-3′ and 5′-GATCCTTATGTGGCCATAATC-3′; *Grk6*, 5′-GTG ACCTAAAGTTCCACAATC-3′ and 5′-CTTTAGATCCCTGTACAC AATG-3′; *Hprt* (control housekeeping gene), 5′-AGGGATTTGAAT CACGTTTG-3′ and 5′-TTTCATGGCAACATCAACAG-3′. For generating NIH 3T3 stable lines with untagged Gpr161, we expressed a codon-wobbled form of mouse Gpr161 cDNA (5′-TCGGTGGAGTTT GATGAG-3′ in frame mutagenized to 5′-TCTGTCGAATTCGAC GAA-3′), and quantitative PCR primers were designed specifically to detect the codon-wobbled form as follows: 5′-TGCCATCGATCGCTA CTACG-3′ and 5′-CACTTGAATTCGTCGAATTCGACAG-3′.

Immunofluorescence and microscopy

Cells were cultured on coverslips until confluent and starved for indicated periods. Cells were treated with respective drugs for the indicated time points before fixation with 4% PFA. When using antibodies against GFP(except in BiFC experiments in Fig. S4), Ptch1, or pan–β-arrestin, the cells were postfixed with methanol for 5 min at −20°C. After blocking with 5% normal donkey serum, the cells were incubated with primary antibody solutions for 1 h at room temperature or overnight at 4°C (anti–pan-β-arrestin; Thermo Fisher Scientific) followed by treatment with secondary antibodies for 30 min along with Hoechst 33342 (Invitrogen). The coverslips were mounted using Fluoromount-G (SouthernBiotech). Images were acquired on an AxioImager.Z1 microscope (ZEISS), a PCO Edge sCMOS camera (BioVision Technologies), and PlanApochromat objectives (10×/0.45, 20×/0.8, 40×/1.3 oil, 63×/1.4 oil), controlled using Micromanager software or a DeltaVision microscope (Applied Precision Ltd.) and powered by SoftWoRx software 4.1 and with a 60×/1.42 objective. Between 8 and 20 z sections at 0.8- to 1-µm intervals were acquired. For quantitative analysis of ciliary localization, stacks of images were acquired from two to five consecutive fields with confluent cells by looking into the DAPI channel, and percentages of Gpr161-positive ciliated cells were counted. Maximal projections from images of stacks were exported from ImageJ/Fiji using a custom written macro (M. Mettlen) using similar parameters (image intensity and contrast) for image files from the same experiment.

GPCR immunoblotting

Methods for GPCR immunoblotting have been described elsewhere (Pal et al., 2015). In brief, cells were harvested by scraping in cold TBS (150 mM NaCl, 50 mM Tris, pH 7.5, 2 mM EDTA, and 1 mM EGTA), lysed in the same buffer supplemented with 1% digitonin, and protease/phosphatase inhibitors, clarified at 16,000 *g* for 10 min, assessed for protein levels and subsequently treated with 2× urea sample buffer (4 M urea, 4% SDS, 100 mM Tris, pH 6.8, 0.2% bromophenol blue, 20% glycerol, and 200 mM DTT) at room temperature for 1 h. Equal amounts of protein were loaded to 4–15% Mini-PROTEAN TGX precast gels (Bio-Rad Laboratories, Inc.) and immunoblotted for GFP and α-tubulin.

BRET assays for measuring cAMP

T-REx-293 cells stably expressing CAMYEL (Jiang et al., 2007) and inducibly coexpressing untagged mouse Gpr161 were grown in polylysine-coated 96-well plates for 24 h followed by induction with 4 µg/ml doxycycline for 12 h. Next, the media was replaced with assay buffer (PBS supplemented with 1 mM IBMX and 4 µg/ml doxycycline) and incubated at 37°C for 45 min. 5 µM coelenterazine-h (NanoLight Technology) was added for the last 10 min, and readings were taken simultaneously with 475-nm/535-nm filters in a Berthold Tristar2 multimode plate reader. Baseline ratio was tracked for 2 min followed by addition of various drugs using injectors, and changes in Rluc/eYFP ratio were monitored for additional 5 min.

Intermolecular BRET assays

T-Rex-293 cells were plated in six-well plates at 800,000 cells/well in 2 ml of media. The next day, cells were cotransfected with varying amounts of WT or mutant Gpr161-eYFP constructs (0.3–3.0 µg/well) and a constant amount of Rluc–β-arrestin1/2 (0.3 µg/well) using BioT transfection reagent (BioLand Scientific). In some assays, cells were also transfected with cDNA expressing WT or mutant Smo (0.1–1 µg/well). Total DNA transfected in each assay was maintained constant by transfecting empty vector. After 24 h, the cells were gently dislodged by resuspending in the preexisting media and transferred to polylysine-coated black 96-well plates at 100 µl/well. For each condition, cells were plated in triplicate in two separate plates. The media was replaced once with complete media 18 h later. After further 6 h, the media was replaced and washed once with PBS. Next, cells were incubated with 5 µM coelenterazine-h in a total of 100 µl PBS/well and incubated for 10 min in a CO_2 incubator at 37°C, avoiding light. Next, readings were taken simultaneously with 475- and 535-nm emission filters in a Berthold Tristar2 multimode plate reader five consecutive times. For each condition, BRET ratio (Em^{535}/Em^{475}) calculated was the mean from two separate plates. Values from each plate were calculated by averaging the values from three wells, and values from each well were the mean of five consecutive readings. Net BRET values were calculated by subtracting the BRET ratio of cells transfected with Rluc–β-arrestin1/2 alone from the $Gpr161^{WT/mutant}$-eYFP/Rluc–β-arrestin1/2 cotransfected wells. $BRET_{50}$ values were computed from titration curves generated by curve fitting using the one-site specific binding option in GraphPad Prism.

Bimolecular fluorescence complementation (BiFC)

Parental IMCD3 or stably expressing $Gpr161^{vl}$-$VN155^{I152L}$ cells were infected with VC155-βarrestin2 expressing retrovirus. The infected cells were selected with the appropriate antibiotics for ∼7 d, grown on coverslips, serum starved, and then immunostained using anti-GFP (red) and anti-AcTub (magenta) antibodies. eVenus N/C-fragment positive cilia (red channel) were scored for eVenus complementation by microscopy. For other experiments, IMCD3 cells were transfected with $Gpr161^{vl}$-$VN155^{I152L}$/$Gpr161^{V158E}$-$VN155^{I152L}$ and VC155-βarrestin2-CLS-HA using Lipofectamine 3000 following the manufacturer's protocol on coverslips in a six-well plate. 7 h after transfection, the media was replaced with starvation media. 24 h after transfection, cells were immunostained using anti-HA (red) and anti-GFP (magenta) antibodies, and imaged by fluorescence microscopy. Transfected cells (HA and GFP positive) were scored for eVenus complementation. eVenus intensity in cilia was quantified using ImageJ.

CD8α-Gpr161 fusion internalization assays

ARPE-19 cells (ATCC) were passaged in each well of a six-well plate (4×10^5/well) and were reverse transfected either with 100 nM control or 50 nM each of two different siRNAs targeting clathrin heavy chain, using Lipofectamine RNAiMAX. Media was replaced 7 h after transfection. 24 h after siRNA transfection, the cells were transfected with CD8α-$Gpr161^{C\text{-}tail}$-LAP5 or CD8α-$Gpr161^{IC3}$-LAP5 constructs

using Lipofectamine 3000. 48 h after siRNA transfection, 2×10^4 cells were transferred to each well of a strip-well 96-well plate. The cells were processed for ELISA, as described before (Reis et al., 2015), using an anti-CD8 antibody targeting the surface glycoprotein (C7423; Sigma-Aldrich). In brief, cells were incubated at 4°C for 1 h to arrest endocytosis of cell surface proteins. This was followed by incubation with anti-CD8 (1:50) antibody at 4°C for 1 h for surface labeling. Cells were then incubated at 37°C for the indicated time points to enable internalization of CD8α proteins bound to antibody. Endocytosis was arrested by putting the cells back to 4°C. Except the control wells, all other wells were subjected to acid wash (0.2 M acetic acid and 0.2 M NaCl), to strip any surface-bound anti-CD8 antibody. This was followed by fixing the cells with 4% PFA, permeabilization with 0.1% Triton X-100, incubation with goat anti–mouse HRP-tagged secondary antibody (Thermo Fisher Scientific), and further developed with OPD (P1526; Sigma-Aldrich). The reaction was stopped with 5M H_2SO_4. Readings were taken at 490 nm using a Biotek Synergy H1 Hybrid plate reader. On completion of ELISA, the cells were subjected to BCA assays for estimating total protein levels. Internalized CD8 fusions were expressed as the % of the respective total surface levels at 4°C (i.e., without acid wash step), measured in parallel, and normalized to total protein levels.

Statistical analyses

Statistical analyses were performed using Student's *t* test for comparing two groups or Tukey's post hoc multiple comparison tests between all possible pairs using GraphPad Prism. Nonparametric Mann–Whitney *U* tests were performed for intensity plots in Figs. 3, S1, and S4 using GraphPad Prism.

Online supplemental material

Fig. S1 illustrates that known Shh pathway agonists do not act as Gpr161 ligands and furthermore, demonstrates that removal of Gpr161 from cilia is dependent on its signaling activity and binding to β-arrestins. Fig. S2 depicts Gpr161 ciliary localization in *Smo*, *Ptch1*, and *Sufu* knockout MEFs and that *Ptch1* up-regulation in *Sufu* knockout MEFs results in increased ciliary levels of Ptch1. Fig. S3 further demonstrates that presence of activated Smo in cilia determines steady-state levels of Gpr161 and also has panels demonstrating Smo trafficking in *β-arrestin* double-knockout MEFs. Fig. S4 further shows that Smo enhances recruitment of β-arrestin to Gpr161 and demonstrates Gpr161^{vl}–β-arrestin binding using BiFC assays. Fig. S5 further illustrates that disappearance of Gpr161 from cilia is dependent on clathrin-mediated endocytosis. In addition, it demonstrates that the lack of removal of Gpr161 has an effect on Shh signaling. Online supplemental material is available at http://www.jcb.org/cgi/content/full/jcb.201506132/DC1.

Acknowledgments

We are thankful for generous gifts of antibodies (Joachim Seeman, Rajat Rohatgi, Kathryn Anderson, Robert Lefkowitz, and Victor Ruiz-Perez), knockout MEFs (Robert Lefkowitz, James Kim, Kathryn Anderson, and Rune Toftgård), and plasmids (Ron Taussig, Paul Sternweis, Lawrence Lum, Jin Jiang, Mark von Zastrow, and Michel Bouvier). We thank Marcel Mettlen (Sandra Schmid laboratory) for writing the macro for importing images from ImageJ and adenovirus reagents. We thank Sandra Schmid, William Snell, and Mike Henne for comments on the manuscript. Phoenix A cells were provided by the Indiana University National Gene Vector Biorepository.

This project was funded by recruitment grants from Cancer Prevention Research Institute of Texas (R1220; S. Mukhopadhyay) and the National Institutes of Health (1R01GM113023-01; S. Mukhopadhyay).

The authors declare no competing financial interests.

Submitted: 29 June 2015
Accepted: 11 February 2016

References

Benmerah, A. 2013. The ciliary pocket. *Curr. Opin. Cell Biol.* 25:78–84. http://dx.doi.org/10.1016/j.ceb.2012.10.011

Benovic, J.L., L.J. Pike, R.A. Cerione, C. Staniszewski, T. Yoshimasa, J. Codina, M.G. Caron, and R.J. Lefkowitz. 1985. Phosphorylation of the mammalian beta-adrenergic receptor by cyclic AMP-dependent protein kinase. Regulation of the rate of receptor phosphorylation and dephosphorylation by agonist occupancy and effects on coupling of the receptor to the stimulatory guanine nucleotide regulatory protein. *J. Biol. Chem.* 260:7094–7101.

Benovic, J.L., H. Kühn, I. Weyand, J. Codina, M.G. Caron, and R.J. Lefkowitz. 1987. Functional desensitization of the isolated beta-adrenergic receptor by the beta-adrenergic receptor kinase: potential role of an analog of the retinal protein arrestin (48-kDa protein). *Proc. Natl. Acad. Sci. USA.* 84:8879–8882. http://dx.doi.org/10.1073/pnas.84.24.8879

Berbari, N.F., A.D. Johnson, J.S. Lewis, C.C. Askwith, and K. Mykytyn. 2008a. Identification of ciliary localization sequences within the third intracellular loop of G protein-coupled receptors. *Mol. Biol. Cell.* 19:1540–1547. http://dx.doi.org/10.1091/mbc.E07-09-0942

Berbari, N.F., J.S. Lewis, G.A. Bishop, C.C. Askwith, and K. Mykytyn. 2008b. Bardet-Biedl syndrome proteins are required for the localization of G protein-coupled receptors to primary cilia. *Proc. Natl. Acad. Sci. USA.* 105:4242–4246. http://dx.doi.org/10.1073/pnas.0711027105

Bonazzi, M., L. Vasudevan, A. Mallet, M. Sachse, A. Sartori, M.C. Prevost, A. Roberts, S.B. Taner, J.D. Wilbur, F.M. Brodsky, and P. Cossart. 2011. Clathrin phosphorylation is required for actin recruitment at sites of bacterial adhesion and internalization. *J. Cell Biol.* 195:525–536. http://dx.doi.org/10.1083/jcb.201105152

Bonifacino, J.S., and J. Lippincott-Schwartz. 2003. Coat proteins: shaping membrane transport. *Nat. Rev. Mol. Cell Biol.* 4:409–414. http://dx.doi.org/10.1038/nrm1099

Chávez, M., S. Ena, J. Van Sande, A. de Kerchove d'Exaerde, S. Schurmans, and S.N. Schiffmann. 2015. Modulation of Ciliary Phosphoinositide Content Regulates Trafficking and Sonic Hedgehog Signaling Output. *Dev. Cell.* 34:338–350. http://dx.doi.org/10.1016/j.devcel.2015.06.016

Chen, M.H., C.W. Wilson, Y.J. Li, K.K. Law, C.S. Lu, R. Gacayan, X. Zhang, C.C. Hui, and P.T. Chuang. 2009. Cilium-independent regulation of Gli protein function by Sufu in Hedgehog signaling is evolutionarily conserved. *Genes Dev.* 23:1910–1928. http://dx.doi.org/10.1101/gad.1794109

Chen, W., X.R. Ren, C.D. Nelson, L.S. Barak, J.K. Chen, P.A. Beachy, F. de Sauvage, and R.J. Lefkowitz. 2004. Activity-dependent internalization of smoothened mediated by beta-arrestin 2 and GRK2. *Science.* 306:2257–2260. http://dx.doi.org/10.1126/science.1104135

Chen, Y., N. Sasai, G. Ma, T. Yue, J. Jia, J. Briscoe, and J. Jiang. 2011. Sonic Hedgehog dependent phosphorylation by CK1α and GRK2 is required for ciliary accumulation and activation of smoothened. *PLoS Biol.* 9:e1001083. http://dx.doi.org/10.1371/journal.pbio.1001083

Chih, B., P. Liu, Y. Chinn, C. Chalouni, L.G. Komuves, P.E. Hass, W. Sandoval, and A.S. Peterson. 2012. A ciliopathy complex at the transition zone protects the cilia as a privileged membrane domain. *Nat. Cell Biol.* 14:61–72. http://dx.doi.org/10.1038/ncb2410

Chong, Y.C., R.K. Mann, C. Zhao, M. Kato, and P.A. Beachy. 2015. Bifurcating action of Smoothened in Hedgehog signaling is mediated by Dlg5. *Genes Dev.* 29:262–276. http://dx.doi.org/10.1101/gad.252676.114

Corbit, K.C., P. Aanstad, V. Singla, A.R. Norman, D.Y. Stainier, and J.F. Reiter. 2005. Vertebrate Smoothened functions at the primary cilium. *Nature.* 437:1018–1021. http://dx.doi.org/10.1038/nature04117

Damke, H., M. Gossen, S. Freundlieb, H. Bujard, and S.L. Schmid. 1995. Tightly regulated and inducible expression of dominant interfering dynamin mutant in stably transformed HeLa cells. *Methods Enzymol.* 257:209–220. http://dx.doi.org/10.1016/S0076-6879(95)57026-8

Doherty, G.J., and H.T. McMahon. 2009. Mechanisms of endocytosis. *Annu. Rev. Biochem.* 78:857–902. http://dx.doi.org/10.1146/annurev.biochem.78.081307.110540

Dorn, K.V., C.E. Hughes, and R. Rohatgi. 2012. A Smoothened-Evc2 complex transduces the Hedgehog signal at primary cilia. *Dev. Cell.* 23:823–835. http://dx.doi.org/10.1016/j.devcel.2012.07.004

Feigin, M.E., B. Xue, M.C. Hammell, and S.K. Muthuswamy. 2014. G-protein-coupled receptor GPR161 is overexpressed in breast cancer and is a

promoter of cell proliferation and invasion. *Proc. Natl. Acad. Sci. USA.* 111:4191–4196. http://dx.doi.org/10.1073/pnas.1320239111

Ferreira, F., M. Foley, A. Cooke, M. Cunningham, G. Smith, R. Woolley, G. Henderson, E. Kelly, S. Mundell, and E. Smythe. 2012. Endocytosis of G protein-coupled receptors is regulated by clathrin light chain phosphorylation. *Curr. Biol.* 22:1361–1370. http://dx.doi.org/10.1016/j.cub.2012.05.034

Francis, S.S., J. Sfakianos, B. Lo, and I. Mellman. 2011. A hierarchy of signals regulates entry of membrane proteins into the ciliary membrane domain in epithelial cells. *J. Cell Biol.* 193:219–233. http://dx.doi.org/10.1083/jcb.201009001

Garcia-Gonzalo, F.R., K.C. Corbit, M.S. Sirerol-Piquer, G. Ramaswami, E.A. Otto, T.R. Noriega, A.D. Seol, J.F. Robinson, C.L. Bennett, D.J. Josifova, et al. 2011. A transition zone complex regulates mammalian ciliogenesis and ciliary membrane composition. *Nat. Genet.* 43:776–784. http://dx.doi.org/10.1038/ng.891

Garcia-Gonzalo, F.R., S.C. Phua, E.C. Roberson, G. Garcia III, M. Abedin, S. Schurmans, T. Inoue, and J.F. Reiter. 2015. Phosphoinositides Regulate Ciliary Protein Trafficking to Modulate Hedgehog Signaling. *Dev. Cell.* 34:400–409. http://dx.doi.org/10.1016/j.devcel.2015.08.001

Goetz, S.C., and K.V. Anderson. 2010. The primary cilium: a signalling centre during vertebrate development. *Nat. Rev. Genet.* 11:331–344. http://dx.doi.org/10.1038/nrg2774

Goodman, O.B. Jr., J.G. Krupnick, F. Santini, V.V. Gurevich, R.B. Penn, A.W. Gagnon, J.H. Keen, and J.L. Benovic. 1996. Beta-arrestin acts as a clathrin adaptor in endocytosis of the beta2-adrenergic receptor. *Nature.* 383:447–450. http://dx.doi.org/10.1038/383447a0

Green, J.A., C.L. Schmid, E. Bley, P.C. Monsma, A. Brown, L.M. Bohn, and K. Mykytyn. 2015. Recruitment of β-Arrestin into Neuronal Cilia Modulates Somatostatin Receptor Subtype 3 Ciliary Localization. *Mol. Cell. Biol.* 36:223–235.

Gurevich, V.V., and E.V. Gurevich. 2006. The structural basis of arrestin-mediated regulation of G-protein-coupled receptors. *Pharmacol. Ther.* 110:465–502. http://dx.doi.org/10.1016/j.pharmthera.2005.09.008

Hamdan, F.F., Y. Percherancier, B. Breton, and M. Bouvier. 2006. Monitoring protein-protein interactions in living cells by bioluminescence resonance energy transfer (BRET). *Curr. Protoc. Neurosci.* Chapter 5:Unit 5.23.

Homan, K.T., E. Wu, M.W. Wilson, P. Singh, S.D. Larsen, and J.J. Tesmer. 2014. Structural and functional analysis of g protein-coupled receptor kinase inhibition by paroxetine and a rationally designed analog. *Mol. Pharmacol.* 85:237–248. http://dx.doi.org/10.1124/mol.113.089631

Hu, Q., L. Milenkovic, H. Jin, M.P. Scott, M.V. Nachury, E.T. Spiliotis, and W.J. Nelson. 2010. A septin diffusion barrier at the base of the primary cilium maintains ciliary membrane protein distribution. *Science.* 329:436–439. http://dx.doi.org/10.1126/science.1191054

Humke, E.W., K.V. Dorn, L. Milenkovic, M.P. Scott, and R. Rohatgi. 2010. The output of Hedgehog signaling is controlled by the dynamic association between Suppressor of Fused and the Gli proteins. *Genes Dev.* 24:670–682. http://dx.doi.org/10.1101/gad.1902910

Jackson, A.L., J. Burchard, D. Leake, A. Reynolds, J. Schelter, J. Guo, J.M. Johnson, L. Lim, J. Karpilow, K. Nichols, et al. 2006. Position-specific chemical modification of siRNAs reduces "off-target" transcript silencing. *RNA.* 12:1197–1205. http://dx.doi.org/10.1261/rna.30706

Jiang, L.I., J. Collins, R. Davis, K.M. Lin, D. DeCamp, T. Roach, R. Hsueh, R.A. Rebres, E.M. Ross, R. Taussig, et al. 2007. Use of a cAMP BRET sensor to characterize a novel regulation of cAMP by the sphingosine 1-phosphate/G13 pathway. *J. Biol. Chem.* 282:10576–10584. http://dx.doi.org/10.1074/jbc.M609695200

Kim, J., M. Kato, and P.A. Beachy. 2009. Gli2 trafficking links Hedgehog-dependent activation of Smoothened in the primary cilium to transcriptional activation in the nucleus. *Proc. Natl. Acad. Sci. USA.* 106:21666–21671. http://dx.doi.org/10.1073/pnas.0912180106

Kim, J., E.Y. Hsia, J. Kim, N. Sever, P.A. Beachy, and X. Zheng. 2014. Simultaneous measurement of smoothened entry into and exit from the primary cilium. *PLoS One.* 9:e104070. http://dx.doi.org/10.1371/journal.pone.0104070

Koch, W.J., B.E. Hawes, J. Inglese, L.M. Luttrell, and R.J. Lefkowitz. 1994. Cellular expression of the carboxyl terminus of a G protein-coupled receptor kinase attenuates G beta gamma-mediated signaling. *J. Biol. Chem.* 269:6193–6197.

Kodama, Y., and C.D. Hu. 2010. An improved bimolecular fluorescence complementation assay with a high signal-to-noise ratio. *Biotechniques.* 49:793–805. http://dx.doi.org/10.2144/000113519

Koemeter-Cox, A.I., T.W. Sherwood, J.A. Green, R.A. Steiner, N.F. Berbari, B.K. Yoder, A.S. Kauffman, P.C. Monsma, A. Brown, C.C. Askwith, and K. Mykytyn. 2014. Primary cilia enhance kisspeptin receptor signaling on gonadotropin-releasing hormone neurons. *Proc. Natl. Acad. Sci. USA.* 111:10335–10340. http://dx.doi.org/10.1073/pnas.1403286111

Kovacs, J.J., E.J. Whalen, R. Liu, K. Xiao, J. Kim, M. Chen, J. Wang, W. Chen, and R.J. Lefkowitz. 2008. Beta-arrestin-mediated localization of smoothened to the primary cilium. *Science.* 320:1777–1781. http://dx.doi.org/10.1126/science.1157983

Lefkowitz, R.J., J. Pitcher, K. Krueger, and Y. Daaka. 1998. Mechanisms of beta-adrenergic receptor desensitization and resensitization. *Adv. Pharmacol.* 42:416–420. http://dx.doi.org/10.1016/S1054-3589(08)60777-2

Li, B.I., P.G. Matteson, M.F. Ababon, A.Q. Nato Jr., Y. Lin, V. Nanda, T.C. Matise, and J.H. Millonig. 2015. The orphan GPCR, Gpr161, regulates the retinoic acid and canonical Wnt pathways during neurulation. *Dev. Biol.* 402:17–31. http://dx.doi.org/10.1016/j.ydbio.2015.02.007

Loktev, A.V., and P.K. Jackson. 2013. Neuropeptide Y family receptors traffic via the Bardet-Biedl syndrome pathway to signal in neuronal primary cilia. *Cell Reports.* 5:1316–1329. http://dx.doi.org/10.1016/j.celrep.2013.11.011

Lu, Q., C. Insinna, C. Ott, J. Stauffer, P.A. Pintado, J. Rahajeng, U. Baxa, V. Walia, A. Cuenca, Y.S. Hwang, et al. 2015. Early steps in primary cilium assembly require EHD1/EHD3-dependent ciliary vesicle formation. *Nat. Cell Biol.* 17:228–240. http://dx.doi.org/10.1038/ncb3109

Luttrell, L.M., and R.J. Lefkowitz. 2002. The role of beta-arrestins in the termination and transduction of G-protein-coupled receptor signals. *J. Cell Sci.* 115:455–465.

Marchese, A., M.M. Paing, B.R. Temple, and J. Trejo. 2008. G protein-coupled receptor sorting to endosomes and lysosomes. *Annu. Rev. Pharmacol. Toxicol.* 48:601–629. http://dx.doi.org/10.1146/annurev.pharmtox.48.113006.094646

Marley, A., and M. von Zastrow. 2010. DISC1 regulates primary cilia that display specific dopamine receptors. *PLoS One.* 5:e10902. http://dx.doi.org/10.1371/journal.pone.0010902

Marley, A., R.W. Choy, and M. von Zastrow. 2013. GPR88 reveals a discrete function of primary cilia as selective insulators of GPCR cross-talk. *PLoS One.* 8:e70857. http://dx.doi.org/10.1371/journal.pone.0070857

Matteson, P.G., J. Desai, R. Korstanje, G. Lazar, T.E. Borsuk, J. Rollins, S. Kadambi, J. Joseph, T. Rahman, J. Wink, et al. 2008. The orphan G protein-coupled receptor, Gpr161, encodes the vacuolated lens locus and controls neurulation and lens development. *Proc. Natl. Acad. Sci. USA.* 105:2088–2093. http://dx.doi.org/10.1073/pnas.0705657105

Meloni, A.R., G.B. Fralish, P. Kelly, A. Salahpour, J.K. Chen, R.J. Wechsler-Reya, R.J. Lefkowitz, and M.G. Caron. 2006. Smoothened signal transduction is promoted by G protein-coupled receptor kinase 2. *Mol. Cell. Biol.* 26:7550–7560. http://dx.doi.org/10.1128/MCB.00546-06

Mettlen, M., D. Loerke, D. Yarar, G. Danuser, and S.L. Schmid. 2010. Cargo- and adaptor-specific mechanisms regulate clathrin-mediated endocytosis. *J. Cell Biol.* 188:919–933. http://dx.doi.org/10.1083/jcb.200908078

Milenkovic, L., M.P. Scott, and R. Rohatgi. 2009. Lateral transport of Smoothened from the plasma membrane to the membrane of the cilium. *J. Cell Biol.* 187:365–374. http://dx.doi.org/10.1083/jcb.200907126

Molla-Herman, A., R. Ghossoub, T. Blisnick, A. Meunier, C. Serres, F. Silbermann, C. Emmerson, K. Romeo, P. Bourdoncle, A. Schmitt, et al. 2010. The ciliary pocket: an endocytic membrane domain at the base of primary and motile cilia. *J. Cell Sci.* 123:1785–1795. http://dx.doi.org/10.1242/jcs.059519

Moore, C.A., S.K. Milano, and J.L. Benovic. 2007. Regulation of receptor trafficking by GRKs and arrestins. *Annu. Rev. Physiol.* 69:451–482. http://dx.doi.org/10.1146/annurev.physiol.69.022405.154712

Mukhopadhyay, S., X. Wen, B. Chih, C.D. Nelson, W.S. Lane, S.J. Scales, and P.K. Jackson. 2010. TULP3 bridges the IFT-A complex and membrane phosphoinositides to promote trafficking of G protein-coupled receptors into primary cilia. *Genes Dev.* 24:2180–2193. http://dx.doi.org/10.1101/gad.1966210

Mukhopadhyay, S., X. Wen, N. Ratti, A. Loktev, L. Rangell, S.J. Scales, and P.K. Jackson. 2013. The ciliary G-protein-coupled receptor Gpr161 negatively regulates the Sonic hedgehog pathway via cAMP signaling. *Cell.* 152:210–223. http://dx.doi.org/10.1016/j.cell.2012.12.026

Nachury, M.V., A.V. Loktev, Q. Zhang, C.J. Westlake, J. Peränen, A. Merdes, D.C. Slusarski, R.H. Scheller, J.F. Bazan, V.C. Sheffield, and P.K. Jackson. 2007. A core complex of BBS proteins cooperates with the GTPase Rab8 to promote ciliary membrane biogenesis. *Cell.* 129:1201–1213. http://dx.doi.org/10.1016/j.cell.2007.03.053

O'Neill, P.R., and N. Gautam. 2014. Subcellular optogenetic inhibition of G proteins generates signaling gradients and cell migration. *Mol. Biol. Cell.* 25:2305–2314. http://dx.doi.org/10.1091/mbc.E14-04-0870

Ocbina, P.J., and K.V. Anderson. 2008. Intraflagellar transport, cilia, and mammalian Hedgehog signaling: analysis in mouse embryonic fibroblasts. *Dev. Dyn.* 237:2030–2038. http://dx.doi.org/10.1002/dvdy.21551

Ogden, S.K., D.L. Fei, N.S. Schilling, Y.F. Ahmed, J. Hwa, and D.J. Robbins. 2008. G protein Galphai functions immediately downstream of Smoothened in Hedgehog signalling. *Nature.* 456:967–970. http://dx.doi.org/10.1038/nature07459

Omori, Y., T. Chaya, S. Yoshida, S. Irie, T. Tsujii, and T. Furukawa. 2015. Identification of G Protein-Coupled Receptors (GPCRs) in Primary Cilia and Their Possible Involvement in Body Weight Control. *PLoS One.* 10:e0128422. http://dx.doi.org/10.1371/journal.pone.0128422

Pal, K., M. Mathur, P. Kumar, and K. DeFea. 2013. Divergent β-arrestin-dependent signaling events are dependent upon sequences within G-protein-coupled receptor C termini. *J. Biol. Chem.* 288:3265–3274. http://dx.doi.org/10.1074/jbc.M112.400234

Pal, K., H. Badgandi, and S. Mukhopadhyay. 2015. Studying G protein-coupled receptors: immunoblotting, immunoprecipitation, phosphorylation, surface labeling, and cross-linking protocols. *Methods Cell Biol.* 127:303–322. http://dx.doi.org/10.1016/bs.mcb.2014.12.003

Persson, M., D. Stamataki, P. te Welscher, E. Andersson, J. Böse, U. Rüther, J. Ericson, and J. Briscoe. 2002. Dorsal-ventral patterning of the spinal cord requires Gli3 transcriptional repressor activity. *Genes Dev.* 16:2865–2878. http://dx.doi.org/10.1101/gad.243402

Pfleger, K.D., and K.A. Eidne. 2006. Illuminating insights into protein-protein interactions using bioluminescence resonance energy transfer (BRET). *Nat. Methods.* 3:165–174. http://dx.doi.org/10.1038/nmeth841

Philipp, M., G.B. Fralish, A.R. Meloni, W. Chen, A.W. MacInnes, L.S. Barak, and M.G. Caron. 2008. Smoothened signaling in vertebrates is facilitated by a G protein-coupled receptor kinase. *Mol. Biol. Cell.* 19:5478–5489. http://dx.doi.org/10.1091/mbc.E08-05-0448

Pitcher, J.A., R.A. Hall, Y. Daaka, J. Zhang, S.S. Ferguson, S. Hester, S. Miller, M.G. Caron, R.J. Lefkowitz, and L.S. Barak. 1998. The G protein-coupled receptor kinase 2 is a microtubule-associated protein kinase that phosphorylates tubulin. *J. Biol. Chem.* 273:12316–12324. http://dx.doi.org/10.1074/jbc.273.20.12316

Pusapati, G.V., C.E. Hughes, K.V. Dorn, D. Zhang, P. Sugianto, L. Aravind, and R. Rohatgi. 2014. EFCAB7 and IQCE regulate hedgehog signaling by tethering the EVC-EVC2 complex to the base of primary cilia. *Dev. Cell.* 28:483–496. http://dx.doi.org/10.1016/j.devcel.2014.01.021

Reis, C.R., P.H. Chen, S. Srinivasan, F. Aguet, M. Mettlen, and S.L. Schmid. 2015. Crosstalk between Akt/GSK3β signaling and dynamin-1 regulates clathrin-mediated endocytosis. *EMBO J.* 34:2132–2146. http://dx.doi.org/10.15252/embj.201591518

Reiter, J.F., O.E. Blacque, and M.R. Leroux. 2012. The base of the cilium: roles for transition fibres and the transition zone in ciliary formation, maintenance and compartmentalization. *EMBO Rep.* 13:608–618. http://dx.doi.org/10.1038/embor.2012.73

Rohatgi, R., and W.J. Snell. 2010. The ciliary membrane. *Curr. Opin. Cell Biol.* 22:541–546. http://dx.doi.org/10.1016/j.ceb.2010.03.010

Rohatgi, R., L. Milenkovic, and M.P. Scott. 2007. Patched1 regulates hedgehog signaling at the primary cilium. *Science.* 317:372–376. http://dx.doi.org/10.1126/science.1139740

Rohatgi, R., L. Milenkovic, R.B. Corcoran, and M.P. Scott. 2009. Hedgehog signal transduction by Smoothened: pharmacologic evidence for a 2-step activation process. *Proc. Natl. Acad. Sci. USA.* 106:3196–3201. http://dx.doi.org/10.1073/pnas.0813373106

Ruat, M., L. Hoch, H. Faure, and D. Rognan. 2014. Targeting of Smoothened for therapeutic gain. *Trends Pharmacol. Sci.* 35:237–246. http://dx.doi.org/10.1016/j.tips.2014.03.002

Schlunck, G., H. Damke, W.B. Kiosses, N. Rusk, M.H. Symons, C.M. Waterman-Storer, S.L. Schmid, and M.A. Schwartz. 2004. Modulation of Rac localization and function by dynamin. *Mol. Biol. Cell.* 15:256–267. http://dx.doi.org/10.1091/mbc.E03-01-0019

Shalem, O., N.E. Sanjana, E. Hartenian, X. Shi, D.A. Scott, T.S. Mikkelsen, D. Heckl, B.L. Ebert, D.E. Root, J.G. Doench, and F. Zhang. 2014. Genome-scale CRISPR-Cas9 knockout screening in human cells. *Science.* 343:84–87. http://dx.doi.org/10.1126/science.1247005

Shukla, A.K., G.H. Westfield, K. Xiao, R.I. Reis, L.Y. Huang, P. Tripathi-Shukla, J. Qian, S. Li, A. Blanc, A.N. Oleskie, et al. 2014. Visualization of arrestin recruitment by a G-protein-coupled receptor. *Nature.* 512:218–222. http://dx.doi.org/10.1038/nature13430

Sun, X., J. Haley, O.V. Bulgakov, X. Cai, J. McGinnis, and T. Li. 2012. Tubby is required for trafficking G protein-coupled receptors to neuronal cilia. *Cilia.* 1:21.

Svärd, J., K. Heby-Henricson, M. Persson-Lek, B. Rozell, M. Lauth, A. Bergström, J. Ericson, R. Toftgård, and S. Teglund. 2006. Genetic elimination of Suppressor of fused reveals an essential repressor function in the mammalian Hedgehog signaling pathway. *Dev. Cell.* 10:187–197. http://dx.doi.org/10.1016/j.devcel.2005.12.013

Tanowitz, M., and M. von Zastrow. 2003. A novel endocytic recycling signal that distinguishes the membrane trafficking of naturally occurring opioid receptors. *J. Biol. Chem.* 278:45978–45986. http://dx.doi.org/10.1074/jbc.M304504200

Taylor, F.R., D. Wen, E.A. Garber, A.N. Carmillo, D.P. Baker, R.M. Arduini, K.P. Williams, P.H. Weinreb, P. Rayhorn, X. Hronowski, et al. 2001. Enhanced potency of human Sonic hedgehog by hydrophobic modification. *Biochemistry.* 40:4359–4371. http://dx.doi.org/10.1021/bi002487u

Thal, D.M., K.T. Homan, J. Chen, E.K. Wu, P.M. Hinkle, Z.M. Huang, J.K. Chuprun, J. Song, E. Gao, J.Y. Cheung, et al. 2012. Paroxetine is a direct inhibitor of g protein-coupled receptor kinase 2 and increases myocardial contractility. *ACS Chem. Biol.* 7:1830–1839. http://dx.doi.org/10.1021/cb3003013

Torres, J.Z., J.J. Miller, and P.K. Jackson. 2009. High-throughput generation of tagged stable cell lines for proteomic analysis. *Proteomics.* 9:2888–2891. http://dx.doi.org/10.1002/pmic.200800873

Tukachinsky, H., L.V. Lopez, and A. Salic. 2010. A mechanism for vertebrate Hedgehog signaling: recruitment to cilia and dissociation of SuFu-Gli protein complexes. *J. Cell Biol.* 191:415–428. http://dx.doi.org/10.1083/jcb.201004108

Vieira, O.V., K. Gaus, P. Verkade, J. Fullekrug, W.L. Vaz, and K. Simons. 2006. FAPP2, cilium formation, and compartmentalization of the apical membrane in polarized Madin-Darby canine kidney (MDCK) cells. *Proc. Natl. Acad. Sci. USA.* 103:18556–18561. http://dx.doi.org/10.1073/pnas.0608291103

Watanabe, S., T. Trimbuch, M. Camacho-Pérez, B.R. Rost, B. Brokowski, B. Söhl-Kielczynski, A. Felies, M.W. Davis, C. Rosenmund, and E.M. Jorgensen. 2014. Clathrin regenerates synaptic vesicles from endosomes. *Nature.* 515:228–233. http://dx.doi.org/10.1038/nature13846

Wen, X., C.K. Lai, M. Evangelista, J.A. Hongo, F.J. de Sauvage, and S.J. Scales. 2010. Kinetics of hedgehog-dependent full-length Gli3 accumulation in primary cilia and subsequent degradation. *Mol. Cell. Biol.* 30:1910–1922. http://dx.doi.org/10.1128/MCB.01089-09

Wilson, C.W., M.H. Chen, and P.T. Chuang. 2009. Smoothened adopts multiple active and inactive conformations capable of trafficking to the primary cilium. *PLoS One.* 4:e5182. http://dx.doi.org/10.1371/journal.pone.0005182

Yue, S., L.Y. Tang, Y. Tang, Y. Tang, Q.H. Shen, J. Ding, Y. Chen, Z. Zhang, T.T. Yu, Y.E. Zhang, and S.Y. Cheng. 2014. Requirement of Smurf-mediated endocytosis of Patched1 in sonic hedgehog signal reception. *eLife.* 3:3. http://dx.doi.org/10.7554/eLife.02555